NTNU

Norwegian University of
Science and Technology

Hydrate Prevention by Anti-Agglomerants

Parameters Impacting Flow Performance in
Systems Where Hydrates are Present

Gunnar Fagerholt Knudsen

Petroleum Geoscience and Engineering
Submission date: June 2017
Supervisor: Roar Larsen, IGP

Norwegian University of Science and Technology
Department of Geoscience and Petroleum

Problem Description:

The objective of this thesis is to investigate challenges connected to using Anti-agglomerants as a hydrate prevention technique. In particular, how the viscosity in a hydrocarbon flow system is altered with changes to parameters such as hydrate volume fraction, particle size distribution and water cut. This will be done by looking at fundamental rheology theory for suspensions. As a tool to help in this investigation, a MATLAB cold flow simulator developed by SINTEF will be used. The simulator will be modified to fit the objective of this thesis.

ABSTRACT

Natural gas hydrates are crystalline compounds that, under the right pressure and temperature conditions, may form in hydrocarbon pipelines, causing transport complications. Several methods of countering this have been used in the industry, one of them being the injection of anti-agglomerants. Anti-agglomerants do not prevent hydrates from forming, but prevent plugging by effectively dispersing the hydrate particles so that they can flow as a hydrate slurry.

Even if the injected anti-agglomerants should prevent agglomeration and plugging of a pipe, deliverability issues might occur. For a system with high enough viscosity, the pressure drop along a pipeline could be high enough to regard the transportation as unfeasible. In this thesis, the viscosity of a system with a flowing hydrate slurry will be investigated based on specific process parameters. The selected parameters are chosen based on fundamental theory on the flow of suspensions. Their values are chosen to emulate a realistic scenario as accurately as possible. Parameters include the hydrate volume fraction, the particle size distribution, hydrate particle size and water cut.

The different parameters are evaluated using a Matlab simulator provided by SINTEF. The model is developed by SINTEF as an aid for developing subsea oil and condensate fields by the CONWHYP (Conversion of water to hydrate particles) loop concept. Some modifications have been made to the model to simulate the desired system, as well as to how the model presents data.

Simulation results show how all evaluated parameters influence the viscosity or pressure profile of the system. The slurry viscosity seems to be most sensitive to changes to the hydrate volume fraction, with high volume fractions yielding a higher viscosity. Variations to the particle size distribution are also significant, with sensitivity strongly dependent on the hydrate volume fraction. The results show that the viscosity increases with increasing monodispersity. For a uniform sample, the particle size does not influence the slurry viscosity, but will influence the pressure drop due to the change to the slurry friction factor. Results from water cut simulations show that a hydrate slurry system is highly sensitive to changes in the water cut, and corroborates the scientific literature, which states that anti-agglomerants do not perform well at higher water volume fractions.

SAMMENDRAG

Naturgasshydrater er krystallaktige forbindelser som under riktige trykk- og temperaturforhold kan dannes i hydrokarbonførende rørledninger, og som kan føre til transportkomplikasjoner. Flere metoder for å forhindre hydratplugging eksisterer, og en av disse er injeksjon av anti-agglomeranter. Anti-agglomeranter forhindrer ikke hydratdannelse, men forhindrer plugging ved å dispergere hydratpartiklene slik at de kan strømme som en ”hydratslurry”.

Selv om de injeserte anti-agglomerantene greier å forhindre hydratplugging kan man få problemer med leveringsevnen til systemet. For systemer med høy nok viskositet kan trykkfallet langs rørledningen bli så høyt at transporten ikke er økonomisk gunstig. I denne oppgaven har viskositeten til en strømmende hydrat slurry blitt undersøkt basert på utvalgte prosessparametre. Verdien på de utvalgte paramterene ble valgt for å etterlikne et reelt hydrokarbonsystem best mulig. Parametrene inkluderte volumfraksjon hydrat, størrelsesfordeling av partikler, partikkelstørrelse og vann-innhold.

De forskjellige parametrene ble evaluert ved hjelp av en Matlabsimulator utviklet av SINTEF. Modellen har blitt brukt som et hjelpemiddel i utviklingen av subsea olje- og kondensatfelt etter CONWHYP loop-konseptet. Noen modifikasjoner ble gjort for å simulere det ønskede systemet, i tillegg til å endre hvordan modellen presenterer data.

Resultatene viste hvordan alle de evaluerte parametrene påvirket viskositets- eller trykkprofilen til systemet. Slurryviskositeten var tilsynelatende mest sensitiv til endringer i volumfraksjon hydrat, med høyere viskositet ved høyere volumfraksjon. Variasjoner i størrelsesfordeling hadde også signifikante utslag, med en sensitivitet sterkt knyttet til den gjeldende volumfraksjonen med hydrat. Viskositeten økte med økende monodispersitet. For et system med uniform partikkelstørrelse vil ikke diameteren på partiklene påvirke viskositeten. Den vil derimot påvirke trykkprofilen på grunn av endringer i friksjonsfaktoren. Resultatene fra vann-innholdsimuleringen viste at hydratslurrysystemer er svært sensitive til endringer i vann-innholdet, som støtter faglitteraturens enighet om at anti-agglomeranter ikke yter godt ved høyt vann-innhold.

Table of Contents

List of Tables

List of Figures

1 Introduction

In multiphase transport systems in petroleum production, one of the biggest challenges is to ensure an unrestricted flow of hydrocarbons. Formation of solid deposits in the pipeline and equipment is often a risk, with gas hydrates, wax, asphaltenes and scales representing the principal problems. In case of deep subsea transportation, gas hydrates are considered by far the most serious and common problem in flow assurance, due to their rapid formation. Complete plugging of a pipeline due to hydrate formation will lead to loss in production time and may lead to damaged process equipment and risk for human life.

Natural gas hydrates are crystalline compounds in which gas molecules are trapped inside hydrogen-bonded water cages. Elevated pressures and low temperatures favor formation of these hydrates, such as in deep-water operations in the Gulf of Mexico, or in cold climate operations such as in the North Sea. Several techniques to avoid the formation of gas hydrates exist. Maintaining a high temperature throughout the length of the pipeline keeps the system outside the hydrate-forming region. This is an expensive option due to the cost of insulation and/or heating of the pipeline. Another option is to keep a lower system pressure during production. The drawback with this method is the lower transportation efficiency in the pipeline, due to lower fluid density.

Traditionally, injection of methanol or glycol is frequently used to prevent hydrate formation; by altering the thermodynamic conditions for hydrate formation. However, as modern petroleum production advances into deeper and colder production environments, the large volumes of these thermodynamic inhibitors required is very expensive, and might not be economically feasible. Consequently, efforts have been made on trying to replace these thermodynamic inhibitors with the more cost-effective Low Dosage Kinetic Inhibitors (LDHIs). Two types of LDHIs exist; the kinetic inhibitors inhibit the hydrate formation for a long period by extending the duration from the beginning when the system falls into the hydrate-forming region until the onset of hydrate formation.

Anti-agglomerants do not inhibit hydrate formation, but prevents the agglomeration of hydrate crystals into larger, pipe-plugging masses. Instead, the hydrates form small, dispersed particles that are easily suspended and transported in the fluid. However, transportation issues may still occur, as the system viscosity will increase with the presence of hydrate particles in the liquid phase. Even if the pipe does not become completely plugged, the increased pressure drop due to the high viscosity may render the transportation of the hydrocarbons unfeasible.

This paper aims to investigate certain parameters that affect the suspension viscosity. This will be done by looking into the concepts of elemental rheology theory for suspensions. To visualize the effects of these parameters, a MATLAB simulator provided by SINTEF will be modified and used. The programs intended use is to simulate flow of hydrocarbons through a CONWHYP (Conversion Of Water to Hydrate Particles) loop. Modifications include arranging a better read of the viscosity output data, and setting up a script where the parameters in question can be easily changed for efficient comparison of different cases.

Chapter 2 provides the theoretical basis and motivation for the simulations made. Fundamentals of natural gas hydrates are reviewed in chapter 2.1, along with conventional means of preventing hydrate plugging in hydrocarbon flowing systems. Chapter 2.2 reviews anti-agglomerants to more detail, such as their mechanisms, operational range and limitations. Rheology theory is presented in chapter 2.3, providing insight into which parameters might influence the viscosity of suspensions. The last chapters in section 2 are dedicated to explaining the CONWHYP concept, how the Matlab simulator works and which modifications are made to it to make it a practical tool in this thesis. A considerable amount of effort has been devoted to understanding and using the simulator properly, and it is therefore presented in detail.

Simulation results are presented and discussed in section 3, before chapter 4 concludes the work, along with some recommendations for further work.

2 Theoretical Framework

2.1 Natural Gas Hydrates

Natural gas hydrates are crystalline compounds that form when hydrogen-bonded water molecules in a lattice structure (the host) are stabilized by the encapsulation of a gas molecule (the guest). They are often termed clathrates or inclusion compounds, which means that the water molecules form a network of cages that trap the small guest molecules, such as methane or ethane. The formation of hydrates is triggered in an environment where the appropriate amounts of gas and water molecules are present, typically under high pressure/low temperature conditions.

There is a wide range of molecules that have shown to form hydrate gases, with methane, ethane and propane being those of most practical interest. Other common hydrate formers are carbon dioxide and hydrogen sulfide. When hydrates form, water crystallizes to create a lattice of molecular-sized cages that trap the guest molecules (figure 2.1), despite no chemical bonds between the water host and molecule guest.

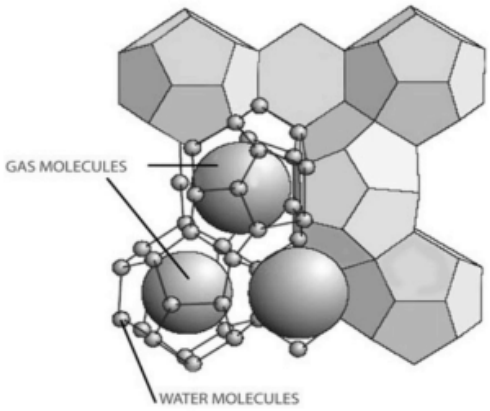

Figure 2.1: Trapping of gas molecules in the gas hydrate particle, with the cages composed of hydrogen-bonded water molecules (Giavarini and Hester, 2011).

The structure of the hydrate crystal is highly dependent on the guest molecule. In contrast to hydrated salts, which exhibit stoichiometry, gas hydrates are non-stoichiometric. In other words, the guest-to-water ratio of the molecules in the hydrate varies based on the conditions under which they were formed. For instance, considering one of the most common gas hydrate structures, structure I (sI), filling all

the cages of the structure with methane would give a ratio of 5.75 H_2O:CH_4. In reality, the filling varies around 6 H_2O:CH_4 (Giavarini and Hester, 2011).

An interesting aspect in the study of gas hydrates is the high energy density they provide due to the high concentration of the gas. For methane, one volume of hydrate contains approximately 160 volumes of gas at standard temperature and pressure conditions (Figure 2.2). Comparing it to traditional fuels shows that it has over two orders of magnitude higher energy density than CH_4 gas, and almost 30% the energy density of CH_4 LNG. A more detailed energy density comparison is given in table 1.

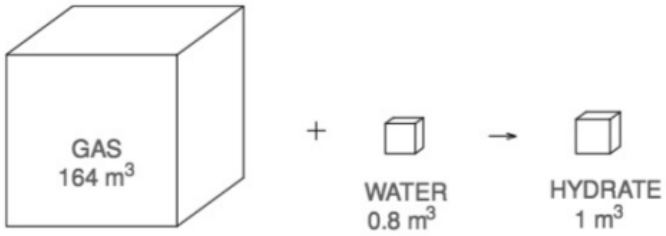

Figure 2.2: Volumetric proportions between water and gas in a methane hydrate.

Combustible	Density (g/ml)	Energy Density (BTU/ft^3)	Energy Density (kJ/m^3)
CH_4 (gas)	6.66×10^{-4}	1,012	37,706
CH_4 (LNG)	0.42	570,000	21.2×10^6
CH_4 (sI hydrate)	0.91	165,968	6.2×10^6
Liquid hydrogen	0.07	229,000	8.5×10^6
Gasoline	0.74	876,000	32.6×10^6
Jet fuel	0.78	910,000	33.9×10^6
Diesel	0.78	995,000	37.1×10^6

Table 1: Energy density comparison of fuels (Max et al., 2006).

This high energy density has made gas hydrates an interesting research topic with regards to storage/transportation of natural gas, as well as energy production from naturally occurring gas hydrates.

2.1.1 Hydrate Prevention

While natural gas hydrates are interesting from an energy resource point-of-view, most efforts are put into handling hydrates that form in pipelines and equipment. Flow assurance of produced hydrocarbons is a critical concern that focuses on designing a system where the fluid can flow uninterrupted from the

producing reservoir to the receiving facility in a safe and secure manner. Formation of solid deposits in the pipeline and equipment is often a risk, with gas hydrates, wax, asphaltenes and scales representing the principle problems. In case of deep subsea transportation, gas hydrates are considered by far the most serious and common problem in flow assurance, due to their rapid formation. Complete plugging of a pipeline due to hydrate formation will lead to loss in production time and may lead to damaged process equipment and risk for human life.

There are essentially three techniques of avoiding gas hydrate plugs in the industry:

- Keeping the system outside the hydrate forming region
- Delaying the hydrate growth for a period longer than pipeline residence time of the fluid
- Allowing for gas hydrates to form, but prohibiting them from agglomerating

The following section will give a brief review on how these techniques are implemented in the industry to avoid hydrate problems, and discuss their respected benefits and drawbacks.

2.1.2 Hydrate Prevention Techniques

Gas hydrate formation will only occur when these three conditions are met:

- Presence of water
- Presence of gas molecules
- High pressure and low temperature

Hydrate prevention eliminates one or more of these conditions, and several methods are available. Water can be removed from the production stream before it enters the transportation pipeline, for instance by having offshore dehydration facilities or a subsea separator. This solution would eliminate the possibility of hydrate formation permanently. However, it is rarely the most cost effective alternative. Removing the gas molecules from the production stream would inarguably eliminate the possibility of hydrate formation, but is obviously not an option, as this would render the production pointless. Reducing the export pressure could move the system out of the hydrate formation region, with the consequence of

decreased gas density (and thereby decreased energy density) of the production stream.

The primary practical means of hydrate formation prevention is hindering the temperature- and pressure profile of the pipeline from entering the hydrate formation region during normal production. This can be done either by narrowing down the hydrate formation region (pushing the hydrate envelope to the left on the P&T-plot) by injecting thermodynamic inhibitors or by insulating and/or heating the flow line.

2.1.2.1 Thermal Methods

As the production flow progresses through a flowline, it will cool toward ambient temperatures and therefore approach the hydrate formation region. Thermal methods include measures such as insulation, upstream heating and burial of the pipeline in order to keep the production profile outside the hydrate formation region. In figure 2.3 and 2.4, two production profiles from a case study of the Dog Lake Field export pipeline in Louisiana (Todd, 1996) are presented to qualitatively display the effect of a combination of the three aforementioned methods.

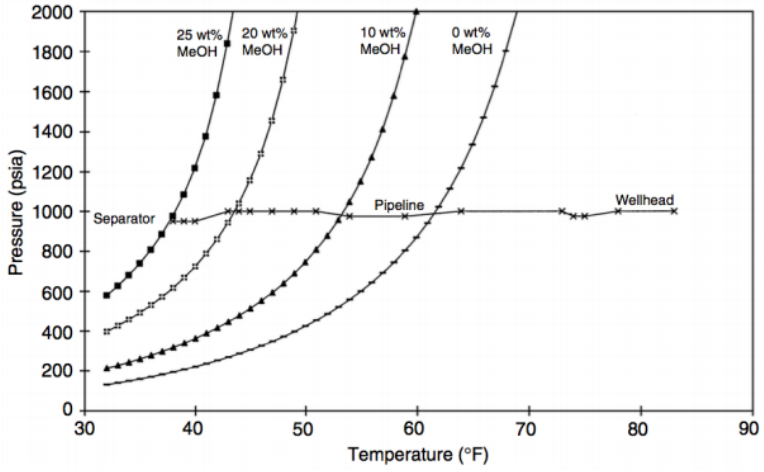

Figure 2.3: Dog Lake flowline conditions with no thermal methods implemented (Todd et al., 1996).

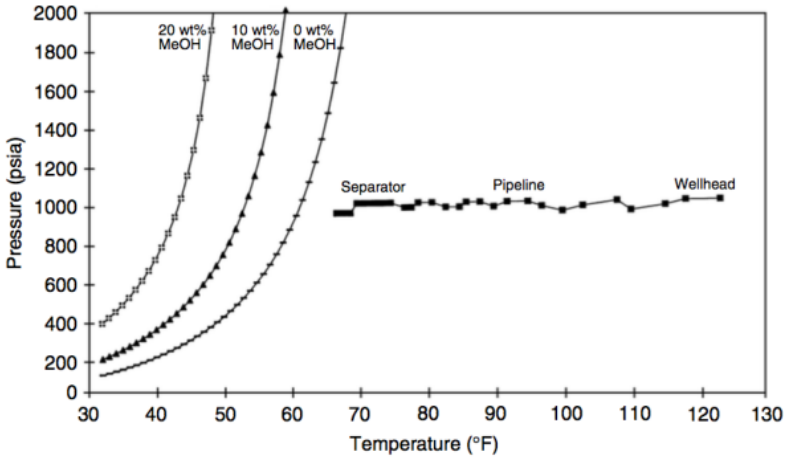

Figure 2.4: Dog Lake flowline conditions with pipeline insulation, heating and burial (Todd, 1996).

Consider the two production profiles with no thermodynamic inhibitor (MeOH) added to the system. It can be seen in figure 2.3, where no thermal methods are implemented, that the system eventually falls well within the hydrate envelope. In figure 2.4 the pipeline has been buried and insulated, and the production stream has been heated at the wellhead. These measures allow the flow to maintain a sufficiently high temperature throughout the length of the pipeline, thereby avoiding entering the hydrate formation region.

2.1.2.2 Thermodynamic Inhibitors (THIs)

As stated in the introduction to this chapter, one method of hydrate prevention is removing water from the production stream directly. Water in the stream can also be removed indirectly, by injecting an inhibitor that forms hydrogen bonds with the free water. Consequently, the concentration of non-hydrogen bonded water is lower, water activity is reduced, and higher pressures and lower temperatures are required for hydrate formation to occur. The change in the system can be seen in figure 2.5, where the hydrate envelope is shifted further to the left with increasing concentration of inhibitor:

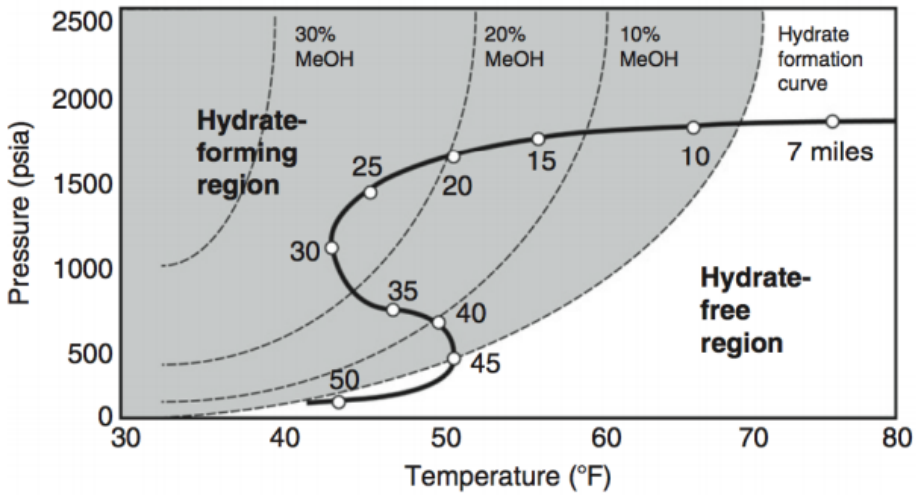

Figure 2.5: Hydrate formation conditions as a function of inhibitor (MeOH) concentration in free water. Flowline conditions are shown at distances along the black curve (Palermo and Sloan, 2011).

From figure 2.5, for the given flowline conditions, it can be estimated visually that the concentration of inhibitor required in the free water to avoid entering the hydrate formation region is approximately 25%.

Methanol (MeOH) and monoethylene glycol (MEG) are among the most frequently used inhibitors in the industry (Palermo and Sloan 2011). Because of their difference in molecular mass, they are injected differently. Methanol, with its low molecular mass, is vaporized into the gas phase and flows to a point of free water accumulation mixed with this gas phase. MEG is usually injected as liquid to inhibit hydrates in the aqueous phase and dissolve in water adsorbed at the water-wet flowline wall. Figure 2.6 shows typical values for reduction in hydrate formation temperature at different fractions of inhibitor in the aqueous phase for methanol and MEG.

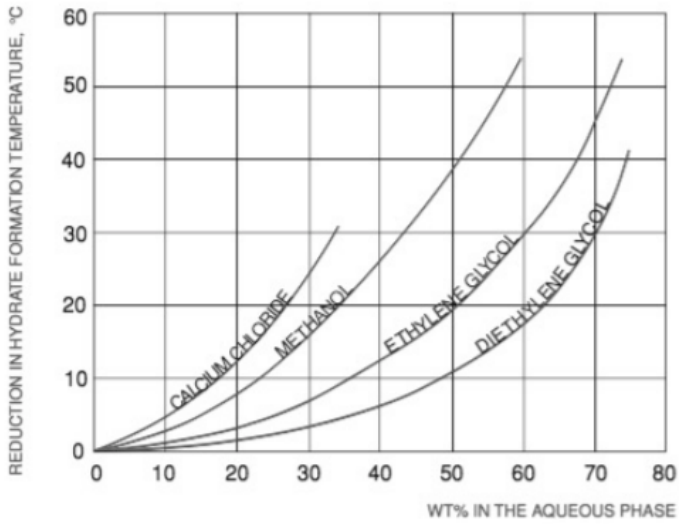

Figure 2.6: wt. % in the aqueous phase vs reduction in hydrate formation temperature for different inhibitors (Giavarini and Hester, 2011).

Due to its effectiveness and low cost, methanol is a widely used inhibitor. However, there are many drawbacks when using methanol as an inhibitor. The inhibition process might require a huge volume, it is flammable, relatively volatile, toxic, and exhibits low biodegradability. Only a certain amount of the methanol injected will actually contribute to inhibition, as it tends to partition more into the hydrocarbon phase than for instance glycol. In addition, downstream refineries often have restrictions on methanol concentrations entering their facilities. Violating these restrictions might lead to significant economic losses. A comparison of the advantages and disadvantages of methanol and MEG is presented in table 2.

Hydrate inhibitor	Methanol (MeOH)	Monoethylene glycol (MEG)
Advantages	Easily vaporized into gas For flowline and topside plugs No salt problems	Relatively recoverable For plugs in wells and risers Low gas and condensate solubility
Disadvantages	Costly to recover High gas and condensate losses Poisons molecular sieves, catalysts; downstream problems	High viscosity inhibits flow Boiler fouling, salt precipitation

Table 2: MeOH and MEG attributes comparison (Sloan, 2000).

2.1.2.3 Low-Dosage Hydrate Inhibitors (LDHI)

The oil and gas industry moves toward increasingly challenging exploration and production conditions. Deeper and colder waters mean higher pressures and lower temperatures, demanding higher effectiveness from the inhibitors injected to prevent hydrate formation. Such conditions will in most cases make injection of thermodynamic inhibitor economically unfeasible, considering the high inhibitor volumes, expensive storage, injection, and regeneration facilities that would be required. These issues led to the search for other methods to prevent gas hydrate formation, and eventually the development of the Low Dosage Hydrate Inhibitors (LDHI) in the nineties (Kelland, 2009). The LDHIs are divided into two classes, namely kinetic hydrate inhibitors (KHIs) and anti-agglomerants (AAs).

KHIs are polymers with low molecular weight that work by bonding to the surface of the hydrate. It is first dissolved in a transportation solvent and then injected into the water phase in a flowline. This prevents any significant nucleation and growth of the hydrate crystal for a period exceeding the residence time in a pipeline. The inhibitor in the water is removed at the end of the pipeline.

Compared to thermodynamic inhibitors such as methanol, KHIs are injected at low concentrations. While THIs are often injected at 20-60 wt. %, KHIs rarely exceed 1 wt. %. In a field in the North Sea where the mono ethylene glycol system was replaced with a kinetic inhibitor system, CAPEX saving were estimated to $40 million USD (Phillips and Grainger 1998).

AAs are surface-active chemicals that do not prevent the formation of hydrate crystals. As the name suggests, it prevents the crystals from agglomerating, by keeping the particles small and well dispersed so that the viscosity of the fluid remains low and the hydrates can be transported along with the produced fluids. At the end of the flowline, the emulsion is broken and water is removed in a separator. Compared to KHIs, AAs are relatively independent of time and appear to be more effective at more extreme conditions (Frostman, 2000).

2.2 Anti-Agglomerants

2.2.1 AA mechanisms

Two subclasses of AAs exist, namely pipeline AAs and gas-well AAs. Common for all AAs is that they allow for hydrates to form but prevent them from agglomerating and accumulating into large masses. A pipeline AA enables the hydrates to form as transportable slurry of hydrate particles dispersed in the liquid hydrocarbon phase. Gas-well AAs on the other hand disperse these particles in an excess of water.

2.2.1.1 Emulsion pipeline AAs

Pipeline AAs can again be divided into two classes based on through which mechanism the AA effect is accomplished. One mechanism is the injection of a surfactant that forms a water-in-oil emulsion. The emulsion confines hydrates to form within the water droplets, thereby prohibiting hydrate agglomeration. The end product is a slurry of hydrate particles suspended in the hydrocarbon phase. Based on the water phase, the dosage levels are around 0.8-1.0 wt. % (Kelland, 2009).

Emulsion Pipeline AAs can be recycled. In 1998, Rojey et al. filed a patent on behalf of the IFP that described an invention that related to a process of transporting a fluid containing a gas phase and water, under conditions where hydrates may form. In the patent, it is explained how the mixture consisting of the liquid hydrocarbon fraction and of the additives in solution is separated and recycled at least partly to a point of the pipe (Rojey et al., 1998). The mixture can be separated as follows:

1. At the pipe outlet, the gas phase is at least partly separated from the rest of the mixture comprising of the liquid hydrocarbon fraction and the additives in solution, the hydrates possibly formed during transportation and the water.

2. The hydrates formed are dissociated so as to obtain a gas phase and an aqueous phase. Then, after dissociation, the gas phase and the aqueous phase are separated from the liquid hydrocarbon phase containing the additive.

3. The liquid hydrocarbon phase containing the additive, or at least part of it, is recycled back to a point of the pipe.

The option of additive recycling is a great advantage as it reduces operational costs and the environmental impact made by the chosen chemical. However, there are a couple of drawbacks to the emulsion AA technology. The first is that the water phase has to be thoroughly emulsified prior to entering hydrate-forming conditions. Otherwise, hydrate agglomeration and deposition is likely to occur. Guaranteeing this emulsification is challenging in the field. Second, during laminar flow or shut down, hydrates form from condensed water on the upper walls of the pipe.

Pilot and field trials have been carried out with emulsion pipeline AAs with mixed success. No full field applications have been carried out. Based on available literature, it seems that most work on this class AA has been disbanded in favor of the hydrate-philic Pipeline AAs, which will be reviewed in the following section.

2.2.1.2 Hydrate-philic Pipeline AAs

The second mechanism by which pipeline AAs work is the one discovered by Shell in the early nineties, where the surfactant molecule has a hydrate-philic head group and a hydrophobic tail (figure 2.7). As many of these surfactant molecules attach to the surface of the hydrate crystal, the crystal becomes hydrophobic and further growth is prevented. The crystals are then easily dispersed in the liquid hydrocarbon phase.

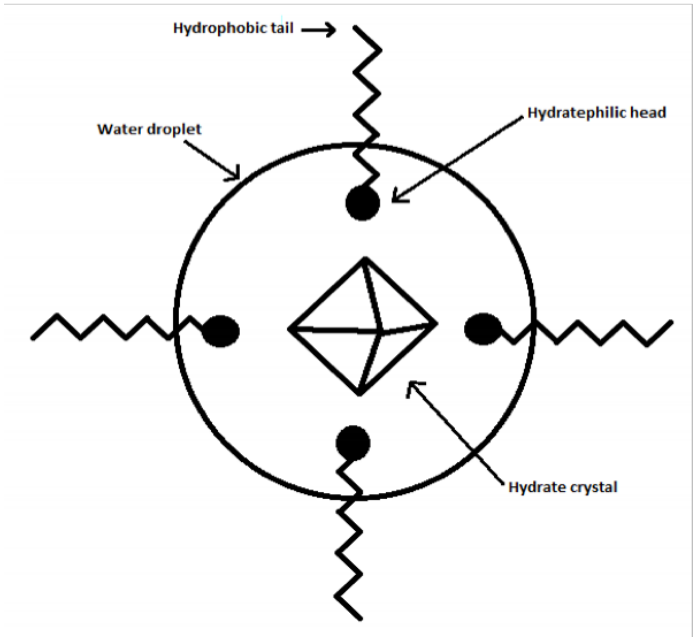

Figure 2.7: Conceptual illustration of AAs interacting with hydrate crystal

While many classes of surfactants have been shown to have hydrate-philic AA properties, the only class that has been commercialized and is in use today is the quaternary ammonium surfactants (QAS) with head groups that in most cases contain two or more n- butyl, n-pentyl or iso-pentyl groups. It has been proven that the butyl or pentyl groups in the quaternary AAs penetrate open cavities and get embedded in the hydrate crystal, preventing the surfactants from detaching (Kelland, 2009). This may be the reason they work better than other surfactants that only interact with the hydrate surface but does not get embedded. In commercial pipelines, butyl groups rather than pentyl groups are used, due to the ease of manufacturing and cost (Kelland, 2009).

2.2.2 Comparing the two classes of LDHIs

A common advantage of using KHIs and AAs in flow assurance is the low concentration needed for adequate inhibition of a system (as the name LDHI suggests). When injected, the concentration of LDHIs rarely exceeds 1 wt. %. Further comparison shows that the applicability of the two techniques differ greatly, wherein one might exhibit advantages where the other has limitations. Most chemicals have both advantages and disadvantages in their use, and AAs and KHIs are no exception.

2.2.2.1 Operational range

KHIs are polymers that work by inhibiting hydrate formation in the water phase only, and they are therefore water-soluble and dispersible. They will be affected by interactions in the bulk water phase or water interfaces so they appear not to be dependent on the water cut. This is a useful attribute, as a usual trend when producing a field is that the water cut increases as the field is produced. The inhibitor injection rate can the easily be adjusted according to the water cut to maintain the same inhibitor effect, given that all other parameters remain the same. In contrast, AA effectiveness is affected by the water cut. At water cuts less than 50%, no significant increase in fluid viscosity is expected, but at higher water cuts, the dispersed hydrate crystals may cause an increase in the viscosity of the liquid hydrocarbon phase and may restrict the flow of the hydrate slurry. A limit to the use of AAs is therefore sufficiently high oil cut of ca. 50-70% (Mehta et al., 2003).

On a general basis, AAs are able to handle a higher degree of subcooling and longer shut-in durations than KHIs developed to date. In deepwater requirements, the

subcooling can be as high as 25 °C. In such conditions, the performance of state-of-the-art KHIs is insufficient. The inhibition effect will be lost relatively early, as the inhibition effect of KHIs is dependent on the degree of subcooling. They can only be used in applications down to ca. 6-7°C subcoolings in long distance pipeline transportation (Kelland et al., 1995). KHIs are therefore rarely the right choice in well production shut-ins, start-ups or deepwater operations. That being said, KHIs are far from structurally optimized, and classes that can handle higher subcoolings might be discovered in the future. AAs, on the other hand do not exhibit degree of subcooling dependency, as AAs allow hydrates to form as very fine crystals dispersed in the hydrocarbon phase. Hence, they are the preferred method for such operations. An exception to this might be faced at extreme subcoolings, where the driving force for hydrate formation may be so high that the rate of hydrate formation surpasses the AAs ability to effectively separate hydrate particles. Figure 2.8 shows theoretical pressure-temperature limitations for the use of KHIs and AAs.

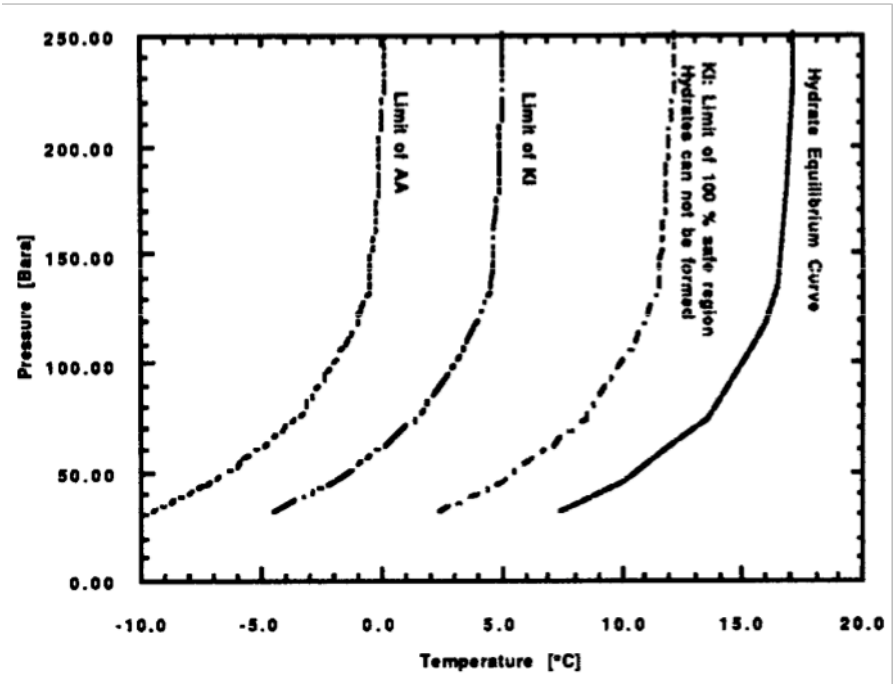

Figure 2.8: PT operating regions for kinetic inhibitors and anti-agglomerants (Dirdal, 2013).

2.2.2.2 Environmental aspects

Beside the limitations in KHI performance, they are a far more environmental friendly alternative than AAs. In the North Sea, tests have been performed to assess the environmental impact of the commercial KHIs poly[VIMA/CAP], with the results that these present no harm to marine lives. In the UK OCNS (Offshore Chemical

Notification Scheme) system, these chemicals are categorized with the grade "E", which is the most environmentally friendly rating. In the Gulf of Mexico, the same chemicals were tested for its toxicity on two marine species. Neither lethal nor sublethal effects were observed at or below the critical dilution of 3.5%, which is a factor determined by platform location, discharge rate, etc. Most of the platforms in the Gulf of Mexico operate with a critical dilution factor of 2% or less, suggesting that water treated with poly[VIMA/CAP] can be safely discharged to sea without any harmful effect to the marine environment (Fu et al., 2001).

2.2.3 AA performance and limitations

Ignoring the environmental impact of anti-agglomerants, it is clear that they represents a highly effective way of handling hydrate plugging issues. They can handle high subcoolings, long shut-in periods, and can produce flowable hydrate slurries over a wide range. However, even if the AAs successfully prevent hydrate plugs from forming, increases in the slurry viscosity may still be a crucial factor when determining whether the operation is feasible or not. Increasing viscosity results in a higher pressure gradient throughout a pipeline. For many transportation pipelines, especially longer pipelines, this increased pressure drop may be too large to effectively transport the fluid from a source to a processing facility. It is therefore important to assess the factors that impact the viscosity of the flowing medium in a flowline where hydrates are present. One of these factor is the water cut, where at higher water cuts, the dispersed hydrate crystals may cause an increase in the viscosity of the liquid hydrocarbon phase and may restrict the flow of the hydrate slurry. Further, research has shown that the hydrates volume fraction, the continuous liquid phase viscosity and the dispersion degree of hydrate particles in the slurry are critical factors that affect the viscosity of natural gas hydrates slurry (Shi et al., 2015). In the following chapter more of these factors are presented through fundamental rheology theory for flow of suspensions.

2.3 Rheology Theory

The study of the physics of continuous materials is called continuum mechanics and constitutes two disciplines:

Fluid mechanics is the study of the physics of continuous materials that deform when a force is applied, and categorizes a fluid as either Newtonian or non-Newtonian. Newtonian fluids exhibit viscosity behavior independent of strain rate. Non-Newtonian fluids viscosity changes with the strain rate. Only a small group of fluids exhibit Newtonian behavior, the most common being fluids such as water, milk, air and alcohol.

Solid mechanics is the study of the physics of continuous materials with a defined rest shape, and categorizes a material as either plastic or elastic. Elastic materials return to their rest shape when relieved from any applied stress, whereas plastic materials permanently deform after a sufficient stress is applied.

Rheology is the study of materials with both solid and fluid characteristics by uniting the seemingly unrelated fields of plasticity and non-Newtonian fluids. It applies to substances with complex microstructure, such as sludges, polymers and suspensions.

2.3.1 The Flow of Suspensions

Structured liquids that we use and encounter in everyday life are very often suspensions/dispersions[1] of particles in a liquid. Products such as mayonnaise, creams and cement are all suspensions. Experience with handling these products tells us that increasing the concentration of the dispersed particles will increase the viscosity of the mixture. For instance, adding flour to water will shift the water from a free flowing liquids, to a paste, and eventually to a soft solid as we continue to add flour. What we need to investigate is, which characteristics of the liquids phase and the added particles influence the change in viscosity. Effect of the particle shape, size, interaction and deformability are all examples of such characteristics, and will be discussed in this chapter.

[1] It is common to differentiate between suspensions and dispersion, where dispersions describes a system made up of small particles so that colloidal factors are not very significant. This differentiation is not made in this paper.

Emulsions are dispersions of deformable liquid drops in a liquid continuous phase. However, if the emulsion consists of very small drops, which exhibit low deformability, they are similar to a small-particle-sized dispersion. As a result, the rules for solid dispersions given below essentially also apply to them.

2.3.2 The continuous phase

Dispersion viscosity is mainly governed by the continuous phase liquid which itself might be Newtonian or non-Newtonian, and then the added dispersed phase where amount, size, shape and deformability of the particles of dispersed material can vary greatly, as well as the interaction between the individual dispersed particles.

In many liquids the continuous phase is Newtonian, like water. Water is a common continuous phase in many household or personal care products. It can also be a Newtonian oil, as in oil-based products such as lubricants and greases.

2.3.3 The effect of low concentrations of particles

Much empirical progress has been made in the study of dispersion, but Albert Einstein was the first to produce important theoretical work in the field. In the beginning of the 20th century, he calculated the viscosity of a dispersion with a very small amount of solid spherical dispersed particles, given by:

$$\eta = \eta_0(1 + [\eta]\phi) \qquad \textbf{2.1}$$

Where η is the measured viscosity and η_0 is the viscosity of the Newtonian continuous phase. [η] is called the intrinsic viscosity, which was calculated to be 2.5 by Einstein. Φ represents the *phase volume*, or that volume of the dispersion that is occupied by the dispersed phase.

2.3.4 The effect of the continuous phase

In all the suspension equations considered here, the viscosity of the suspension is predicted to be directly proportional to that of the continuous phase. This is important to remember, because if any change is made to the continuous phase viscosity (with everything else being equal), the suspension viscosity changes with the same factor. Doubling the continuous phase viscosity will also double the

viscosity of the suspension. This relationship is important when looking at the effect of parameters such as temperature and concentration of additives, to name some.

The following concentrations of, for instance, sodium salts (wt. %) approximately double the viscosity of water at 20°C: Hydroxide (10.5), carbonate (11.5), acetate (15), phosphate (21), sulphate (18), tartrate (19), chloride (25), thiocyanate (35) and nitrate (37). The effect is complex, as it is not a function of molecular weight alone, but also the shape of the dissolved molecules and the way in which they interact with the structure of water. High-weight molecules will have large impact on the viscosity at low addition, as can be observed with dextran (molecular weight 72.000 daltons). Adding at a level of 2.75 wt. % will double the viscosity of water. On the other hand, adding simple organic molecules like glucose will require concentrations of 20+ wt. % to achieve the same effect.

Chemical additives can also decrease the viscosity of water, at least on lower concentrations. It has been demonstrated that some salts of potassium, rubidium, cesium and ammonium produce such a concentration reduction at lower concentrations, and then increasing the viscosity as normal on higher concentrations (Wagner, 1891). This occurs because the salts interfere with the local intermolecular hydrogen bonding of water molecules. One of the biggest decreases is produced by the addition of 36 wt. % ammonium iodide to water at room temperature, where the viscosity decreases by about 13.5%. Figure 2.9 shows the viscosity reduction as a function of mol/L for ammonium chloride, bromide and iodide.

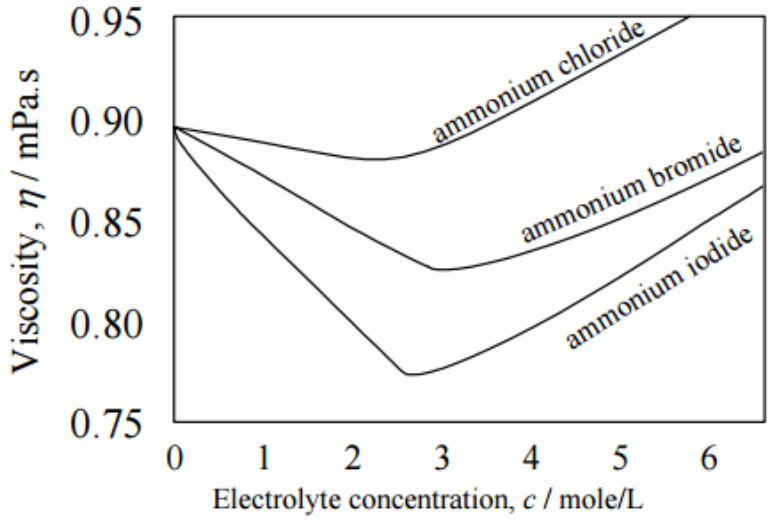

Figure 2.9: Viscosity vs. concentration for some ammonium salt solutions at room temperature (Bancelin, 1911).

With respect to the continuous phase, it is also worth looking at the effect of adding other miscible liquids to water, where the mixture properties are complex, even though the mixture of the same liquid to an organic liquid will give simple mixing. An example of complex mixing is seen in the addition of ethyl alcohol to water. Their individual viscosities are almost the same, but with a very different viscosity when they are mixed together. Figure 2.10 shows this effect.

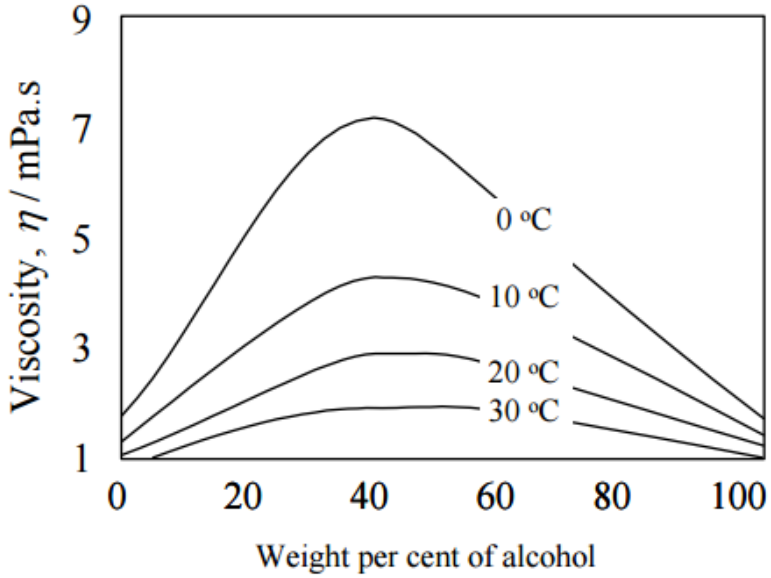

Figure 2.10: Viscosity of water/ethyl-alcohol mixtures for different temperatures (Barnes, 1990).

With all else being equal, the effect of temperature on the overall viscosity is controlled by the viscosity/temperature variation of the continuous phase. The variation of viscosity with temperature for water-based suspensions is around 3% per degree, while oil-based systems can exhibit much higher variations.

2.3.5 The effect of the dispersed phase

The Einstein equation accounts for dispersions with a very small amount of suspended particles. Simply put, this means that the particles are so widely spaced that they do not interact with each other. In reality, this limits a concentration to no more than a few percent phase volume. Bancelin verified the formula experimentally in 1911, by using particles of size 0.3, 1, 2 and 4 μm. No effect of the size of the particle was found (Bancelin, 1911).

While particle size is irrelevant at such low concentrations, the particles shape is not. Viscosity increase comes from the diversion of streamlines in the flow as they are redirected around particles, leading to an increase in viscous energy dissipation,

i.e. viscosity. This extra dissipation increases when the particles are non-spherical, and the incremental amount of viscosity also increases. The measure of this viscosity increase is the intrinsic viscosity [η], which increases when a sphere is pulled out towards a rod, or squashed down towards a disc. Out of the two deformations, the former gives the greater increase in viscosity. A paper-fiber suspension is a typical example of a rodlike particle system, while red blood cells are close to disc-shaped. Simple formulas for both kinds of particles have been derived by Howard A. Barnes (Barnes, 1981) as:

$$[\eta]_{rod} = \frac{7}{100} p^{\frac{5}{3}} \qquad \textbf{2.2}$$

and

$$[\eta]_{disc} = \frac{3}{10} p \qquad \textbf{2.3}$$

for rodlike (prolate) particles and disc-like (oblate) particles, respectively. p is the axial ratio, and is defined in such a way that it is greater than unity.

Additional energy dissipation can be attributed to the presence of electrical charges on the surface of particles, due to flow distorting of the surrounding charge cloud. The effect was accounted for mathematically by Von Smouluchowski as:

$$\eta = \eta_0 (1 + 2{,}5\phi \left\{ 1 + \left(\frac{\epsilon \zeta}{2\pi} \right)^2 \left\{ \frac{1}{2\sigma \eta_0 a^2} \right\} \right\}) \qquad \textbf{2.4}$$

where ϵ is the relative permittivity of the continuous phase, ζ is the electrokinetic potential, σ is the specific conductivity of the continuous phase, and a is the radius of the spherical particles. Here, the size effect is introduced, since the smaller the particle, the larger the effect of the fixed-thickness electrostatic layer relative to the particle size, and hence the greater the effective phase volume.

2.3.6 The effect of medium/high concentrations of particles

Because the Einstein equation only applies to suspensions where particles are not aware of each other's existence, it provides little help for real situations. It did however act as an exact starting point for many following empirical equations, each of which attempted to increase the concentration range into a more practical region. One of the more useful of these equations is the Kreiger-Dougherty (K-D) equation (Barnes, 2000), given by:

$$\eta = \eta_0 \left(1 - \frac{\phi}{\phi_m}\right)^{-[\eta]\phi_m} \qquad \textbf{2.5}$$

where ϕ_m is the *maximum packing fraction*, the concentration where enough particles have been added to the system for the viscosity to become infinite. At rest, this is often near the random close-packing limit of approximately 64%. However, we shall later see that the maximum packing fraction can vary, depending on the circumstances.

In the event of very small phase volume, the K-D equation reduces to the Einstein equation. A very convenient result that has been found experimentally, which shows that the product of $[\eta]\phi_m$ is very often around the value 2. This simplifies the equation to:

$$\eta = \eta_0 \left(1 - \frac{\phi}{\phi_m}\right)^{-2} \qquad \textbf{2.6}$$

with only ϕ_m being the real variable. This variable is a function of particle size distribution (PSD), particle deformability and flow conditions. A wider particle-size distribution will give a higher maximum packing fraction. An example of the effect is illustrated in figure 2.11 for the packing of dry powders (Wakeman, 1975).

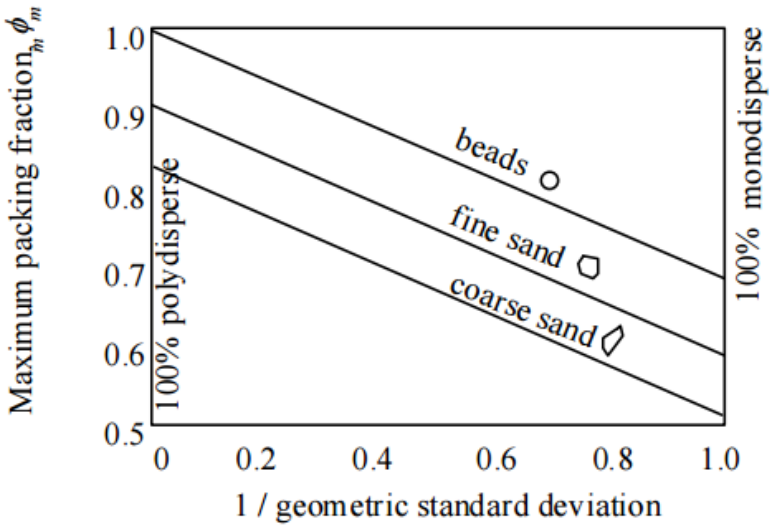

Figure 2.11: The maximum packing fraction of a powder as a function of polydispersity (Wakeman, 1975)

Figure 2.11 also illustrates the same effect for slightly non-spherical particles (the fine sand). The particular kind of size distribution used in this illustration is a 'log normal' kind, and is a consequence of many size-reduction operations such as grinding up of solid particles.

ϕ_m is an important variable to manipulate when trying to control or understand the viscosity of concentrated dispersions. A widening or narrowing of the PSD can be attempted, in order to alter ϕ_m, and consequently getting a different viscosity. If the particles are monodispersed, then mixtures of particle sizes can reduce the viscosity if the size ratio is around 4:1, due to smaller particles occupying the gaps between the larger particles. Figure 2.12 shows how this size-mixing maneuver is effective for higher concentration suspensions. The effect is equally good when mixing three different sizes (as shown in figure 2.13), but becomes impractical when mixing more sizes. This exercise is used in the production of concrete, when as aggregate material possible needs to be added while still making sure the concrete can flow relatively easily.

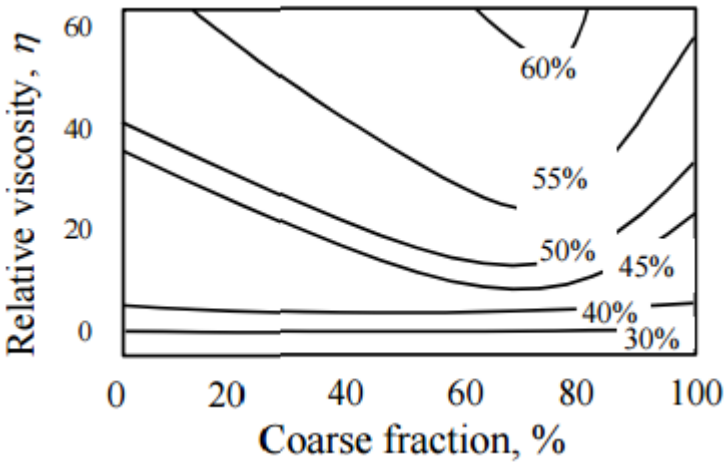

Figure 2.12: Relative viscosity of a binary mixture of particles with size ratio >4:1, for various total phase volumes (Barnes, 2000).

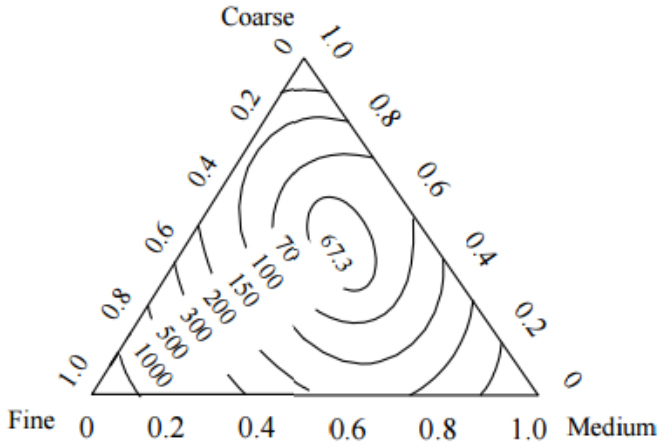

Figure 2.13: Relative viscosity of a ternary mixture of particles in suspension, where the total phase volume is 66% (Barnes et al., 1989).

A brief explanation of how to read the ternary diagram is given in appendix I.

2.3.7 Particle size effects of concentrated dispersions

Spatial arrangement is an important aspect when looking at the effect of particle size of dispersions. At rest, the particles are randomly dispersed throughout the continuous phase due to the Brownian motion in the fluid phase. At low shear rates, a great deal of co-operative movement is required to allow these particles to move in the flow direction while maintaining the overall random distribution, which results in a high viscosity. At higher shear rates, however, particles tend to move from the random arrangement towards aligning into strings and layers, as can be seen in figure 2.14.

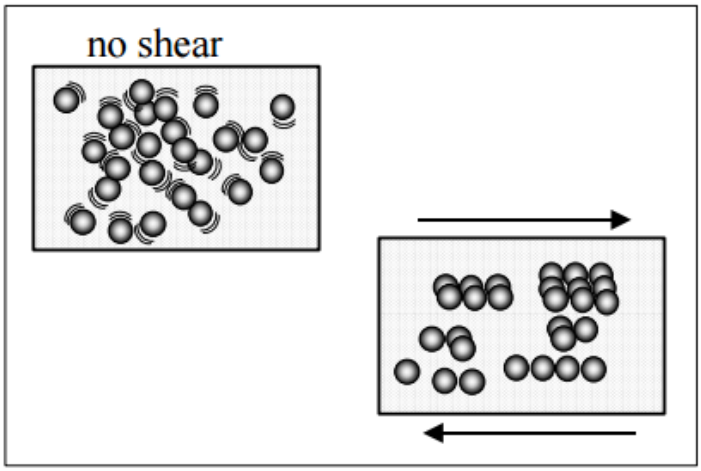

Figure 2.14: Illustration of how particles align in the dispersion when subjected to shear flow (Barnes, 2000).

As the shear rate increases in a system, the average distance between the particles increases in a direction perpendicular to the flow direction, and decreases along the flow direction. This change in spatial arrangement allows the particles to move past each other easier, thus lowering the viscosity. This effect is accounted for in the K-D equation by a small but significant increase in the value of the maximum packing fraction ϕ_m. For a dispersion of monodisperse, spherical particles, typical values of ϕ_m for very low and very high shear rates are 0,62 and 0,72, respectively (Barnes, 2000). While seemingly small, this change produces large effects at high concentrations resulting in a large amount of shear thinning in concentrated suspensions.

The effect of particle size on the viscosity can be attributed to this shear thinning phenomenon. Shear thinning is easier for large particles where Brownian motion is less effective and the shear forces are correspondingly more important. The effect of Brownian motion is longer lasting when a small-particle-sized dispersion is sheared, and higher values of shear rate are needed to obtain the same shear thinning effect. This is illustrated in figure 2.15.

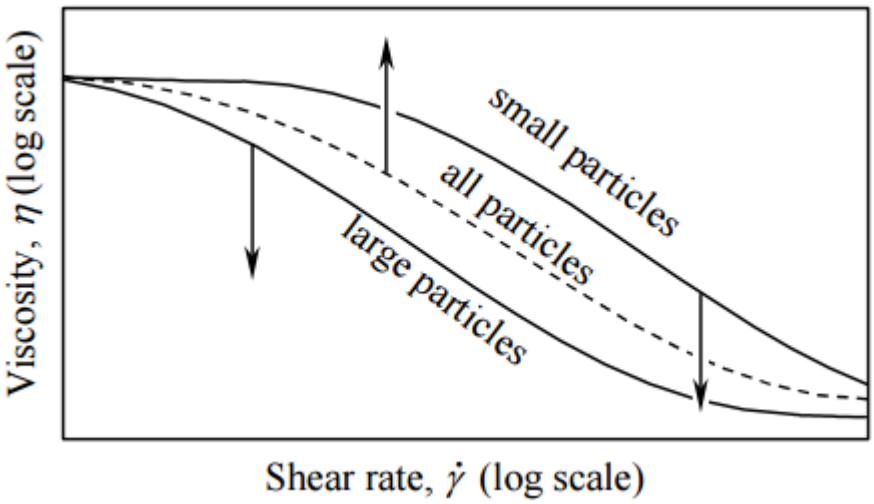

Figure 2.15: Viscosity as a function of the shear rate for large and small particles size suspensions (Barnes, 2000).

2.3.8 Particle shape effects in concentrated dispersions

Depending on the shape of the dispersed particles, different thickening effects will occur. In descending order, different thickening effects can be seen for the shapes

- Rods/fibres
- Plates
- Cubes/grains
- Spheres

when the same phase volume of particles is added to a liquid. The approximate order of thickening power for each shape is presented in figure 2.16, with rods/fibres providing the highest thickening of the shapes. The fibers effect is controlled by the aspect ratio of the particle, as shown in figure 2.17. As we remember from the K-D equation, this effect is accounted for by the intrinsic viscosity $[\eta]$. However, we also remember that even if the intrinsic viscosity for the suspension increases, the maximum packing fraction ϕ_m decreases accordingly, so that the product of the two parameters does not differ greatly from 2 (Barnes, 1989).

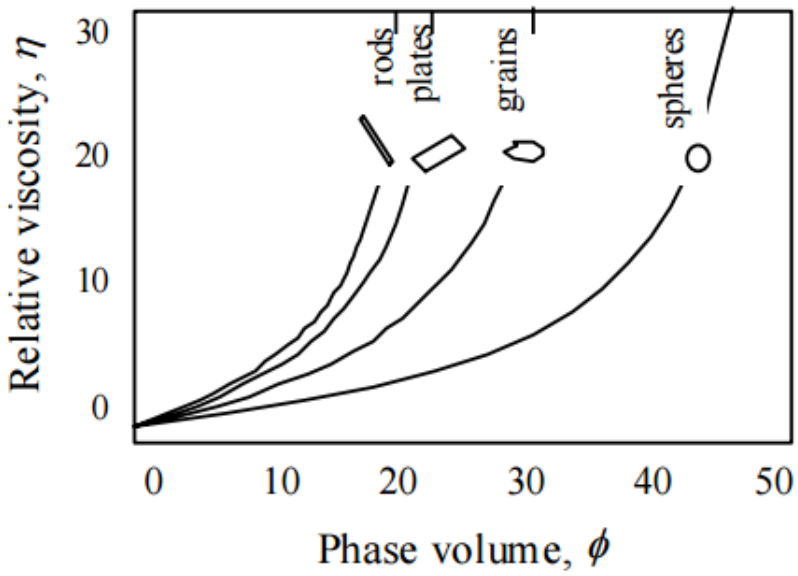

Figure 2.16: Viscosity vs. phase volume for different particle shapes (Barnes, 2000).

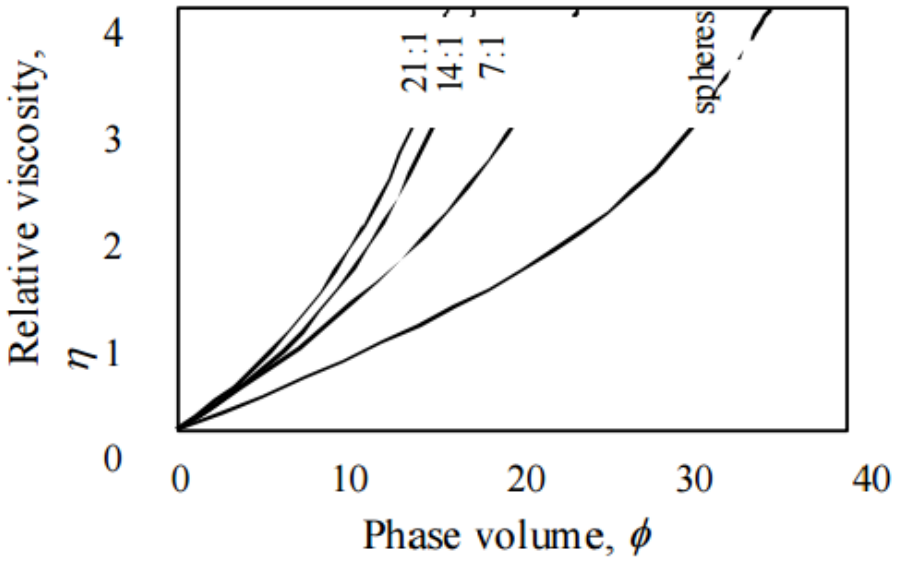

Figure 2.17: Viscosity vs. phase volume for fibres with varying aspect ratio (Barnes, 2000).

The same relationship between the two parameters exists when looking at the particle deformability. For the same amount of dispersed material, the viscosity at high concentrations is lower than the equivalent dispersion of solid particles. Droplets can squeeze past each other during flow and accommodate each other at rest. Thus, the maximum packing fraction is higher, but the intrinsic viscosity is lower.

2.3.9 Particle interactions

The simplest theoretical scenario we can have of any dispersion of submicron particles, is one where the particles in the dispersion are free to get close to and distance themselves from others under the action of the ever-present Brownian motion. This is a scenario where the only resistance the particles have to overcome is when moving through the viscous liquid. However, this is an unrealistic scenario, because significant inter-particle forces are in play, such as van-der-Waals attraction between particles. This attraction force arises from correlated atomic motions in neighboring particles and is always present in all particle-particle interactions.

For the sake of relevance and briefness, these interactions will not be discussed in depth in this paper. These forces are usually significant in the range of 1-10 nanometer sized particles (Barnes, 2000), whereas the particles in question in this paper are usually bigger.

2.4 Cold Flow Technology – Conversion of Water to Hydrate Particles

The Cold Flow Simulator was programmed by SINTEF as a tool in the development of their CONWHYP concept. CONWHYP is short for Conversion of Water to Hydrate Particles, and is a concept where the aim is to convert free water to flowable, "inert" hydrate particles. Achieving this will end hydrate plugging problems and result in better hydrate and corrosion control with less/no chemical additives. It also improves the environmental performance of offshore hydrocarbon production.

SINTEF have developed and tested a pilot system aimed to achieve this goal in a subsea environment close to a wellhead, and have successfully produced dry hydrate particles without excess water, using only specialized flow geometry (Lund and Larsen, 2000). Full scale testing has yet to be conducted.

2.4.1 Hydrate formation and conversion

All mechanisms behind the formation of hydrates are not yet fully understood. It is an established fact, however, that the formation is in practice limited to the macroscopic interface between the water and hydrocarbon phases. After the interface is covered with a hydrate phase, further growth depends on the degree of penetration

of the guest or water species across the hydrate phase. The exact process of this penetration is not well known, but a common assumption in the community is that the hydrate film is penetrated by water through cracks or microperforations (Lund et. al., 1997) (Sugaya and Mori, 1996).

2.4.2 Conversion of gas bubbles in water systems

In a system that eventually enters the appropriate temperature and pressure region for hydrate formation, the first hydrate crystals will develop randomly on the bubble surface in the form of discrete particles. They continue to grow rapidly until the bubble is fully enclosed with a hydrate film. Once fully enclosed, the growth rate slows down to a rate controlled by the degree of penetration of the hydrate layer. Cracks are mainly formed by shrinkage of the bubble as the gas is consumed and penetration occurs due to the capillary pressure exerted by the hydrophilic hydrate surface against the gas phase. Growth rate decreases as the thickness of the layer increases. It is also a function of how agitated the system is. Figure 2.18 shows how the hydrate particles grow into a hydrate layer surrounding the bubble.

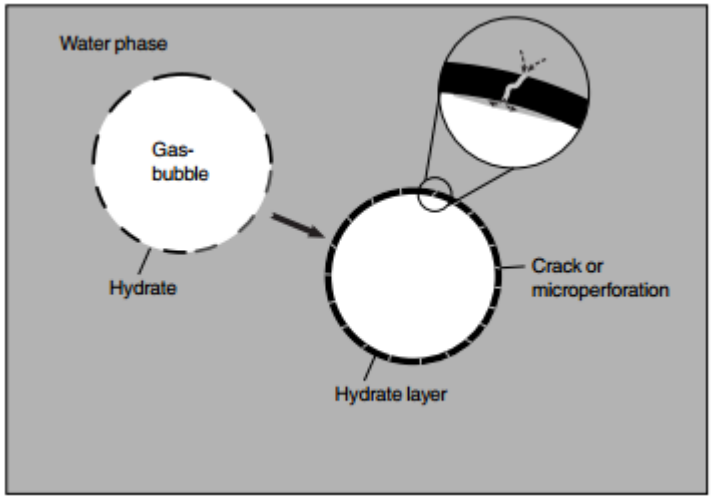

Figure 2.18: The formation and growth of a hydrate layer around a gas bubble (Lund and Larsen, 2000).

Several researchers have reported that, if a hydrodynamic shear is imposed on a hydrate-coated bubble by the surrounding water, particles or flakes of hydrates can shed from the bubble (Lund and Larsen, 2000). These shear forces will create larger cracks in the hydrate layer, as illustrated in figure 2.19.

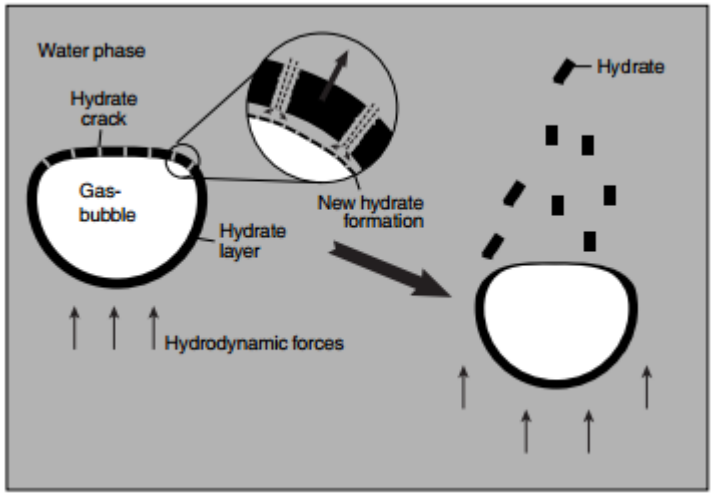

Figure 2.19: Hydrodynamic shear imposed on a gas bubble, causing shedding of hydrate and new hydrate formation (Lund and Larsen, 2000).

Water flows through these cracks and wets the hydrate surface by forming a water film on the hydrate layer. A new hydrate layer then develops on top of this water film, leaving the old hydrate layer fully surrounded by water. The old hydrate layer is then free in the water phase and sheds off the bubble as particles or flakes due to the hydrodynamic shear forces. The driving force for hydrate formation and the magnitude of the shear forces to the bubble is what controls the rate of this process.

2.4.3 Conversion of water droplets in hydrocarbon gas/liquid systems

In gas, oil or condensate phases, hydrate nucleation occurs close to the hydrocarbon phase on a water droplet. Once stable nuclei are formed, the growth continues along the surface of the droplet until it is completely covered with a thin hydrate layer. Water then penetrates outwards from the enclosed water droplet to the hydrophilic hydrate surface against the hydrocarbon phase through cracks in the hydrate film, as illustrated in figure 2.20.

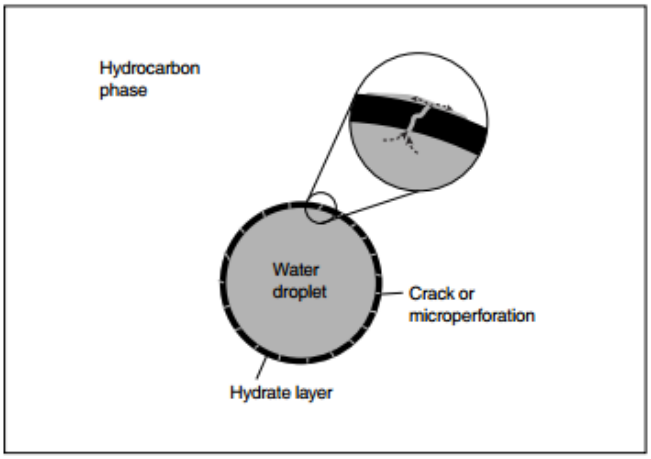

Figure 2.20: Formation and growth of a hydrate on a water droplet in a hydrocarbon gas or liquid system (Lund and Larsen, 2000).

Similar to the gas bubble in the water system, growth rate decreases as the hydrate film thickens, depending on the driving force for hydrate formation and shear forces on the droplets. Further hydrate growth can be triggered in a turbulent system where a water droplet covered by a hydrate film can collide with a pipe or reactor wall to produced larger cracks in the film (figure 2.21). Hydrate forming species on the wall will potentially convert the free water drained from the droplet into new hydrates at a fast rate, often resulting in depositions on the wall.

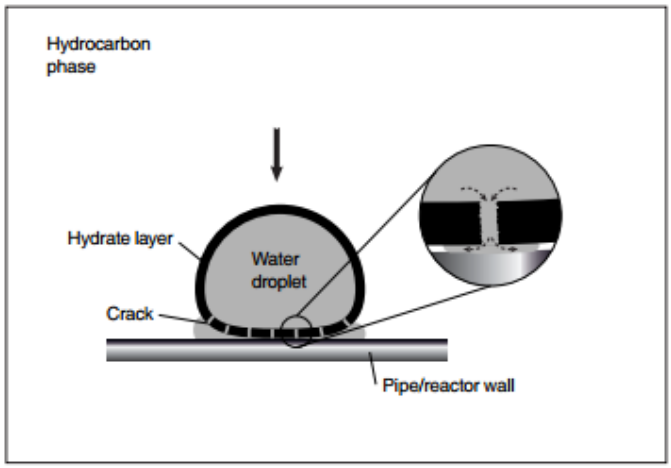

Figure 2.21: Hydrate film covered water droplet colliding with pipe/reactor wall, causing larger cracks and more hydrate forming (Lund and Larsen, 2000).

2.4.4 Conversion of water in turbulent hydrocarbon liquid systems

The process of how water converts into hydrates in turbulent oil or condensate systems varies. However, studies have shown that there are some basic elements in the conversion process where any deviations can be explained by system parameters and fluid compositions. In turbulent liquid systems the water phase is usually distributed in the hydrocarbon phase as unstable water-in-oil emulsions. Initially, hydrates start to grow on the water-hydrocarbon interface, enclosing the droplet with a hydrate film. The hydrate film causes an increase in surface tension, which results in an agglomeration of the droplets in order to decrease the surface area (figure 2.22).

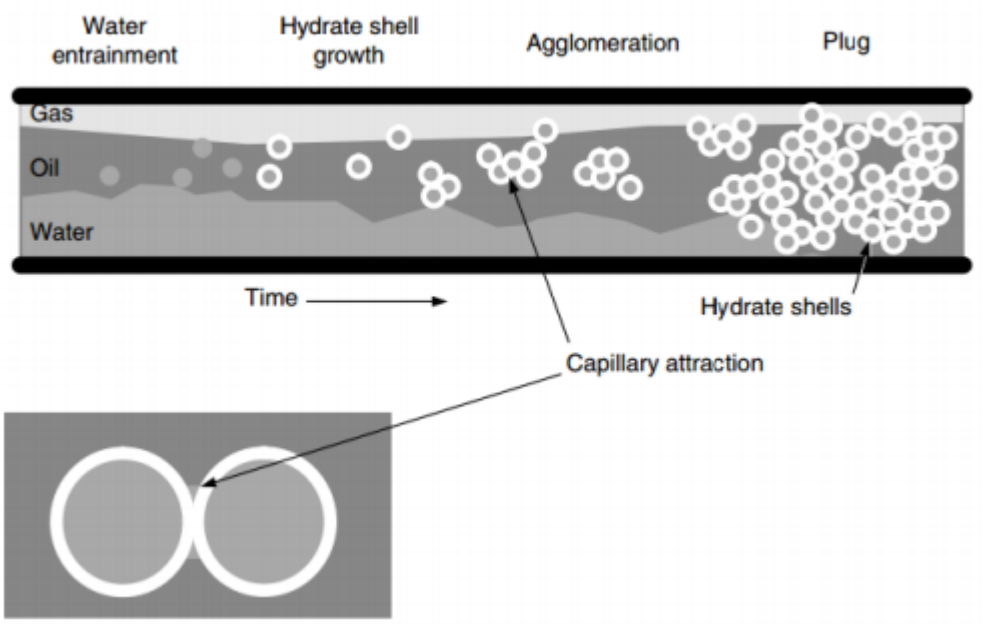

Figure 2.22: Plug formation via aggregation in an oil-dominated system (Sloan, Koh, 2008).

The size, area and form will be under continuous change in a turbulent system. Consequently, new water-hydrocarbon interfaces are created frequently, due to the breakage of the hydrate layer on the hydrate lump. Thus, a turbulent system promotes more rapid hydrate formation. The turbulence also causes formation of small hydrate covered water droplets. The hydrate surface is hydrophilic and will be absorbed in the water lumps, creating a slurry. As the hydrate film on the lumps thicken, the growth rate decreases. However, the turbulent forces will produce cracks in the film, so that free water may be drained from the interior of the water lump and spread on the hydrophilic hydrate layer against the hydrocarbon phase. New hydrates may then form on top of this water, leaving bits of the old hydrate layer completely surrounded by free water (Figure 2.23).

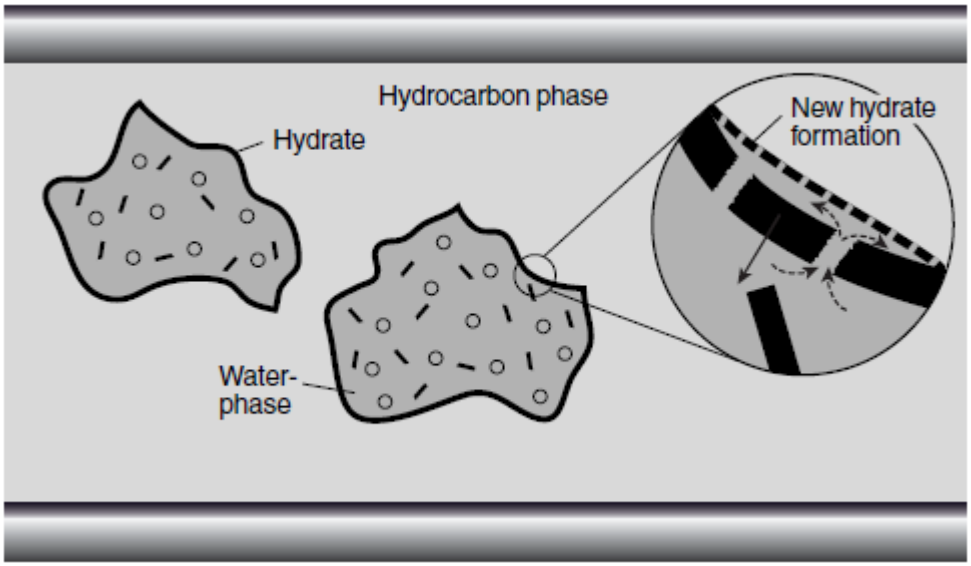

Figure 2.23: Formation of hydrates in a turbulent system. New hydrate forms when free water from the interior of the water lump is drained through cracks in the hydrate film (Lund and Larsen, 2000).

The lump continues to grow until forces between the hydrate particles make the outer area of the lump stiffer. Agglomeration to bigger lumps and plugging may then occur when several of these lumps collide. In the event of a collision, the free water inside the lumps spreads towards the outer hydrate surface, and acts as glue between the lumps.

Further conversion from water to hydrate occurs with transportation of free water from the lump interior by capillary forces through cracks and micro-perforations in the outer layer. This outer layer will increase in thickness until the internal pressure gradients due to capillary forces break them down to smaller hydrate bits, as illustrated in figure 2.24. This break-down process continues until the lumps have been broken down to a powder-like substance, which may still contain up to 30% free water.

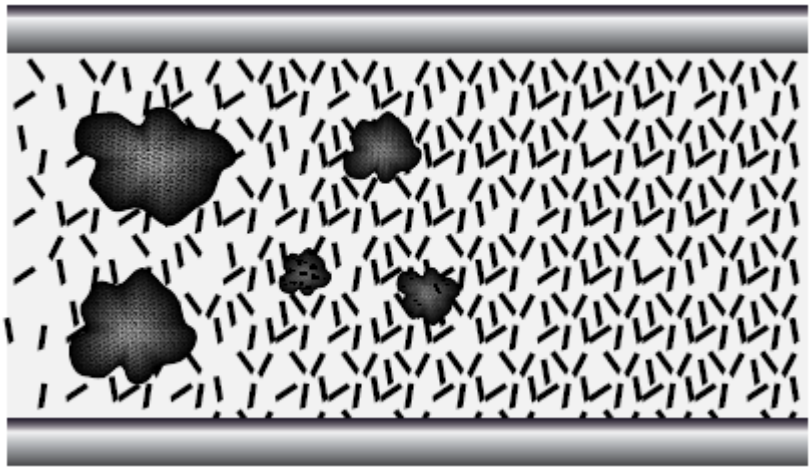

Figure 2.24: Hydrate lumps breaking down into smaller hydrate bits (Lund and Larsen, 2000).

2.4.5 The CONWHYP concept

The main issue when transporting hydrate slurry in a pipeline from a subsea oil or condensate field is the free water present in the hydrates. As explained in the previous section, this free water will contribute to hydrate agglomeration and depositions on the pipe wall, which will eventually create flow restrictions and plugging. The concept of cold flow technology is to actively convert this free water to hydrates near the well in a fast and controlled manner, without any deposition-prone intermediate stages. This is done without chemical additives, only taking advantage of the high degree of hydrophilic behavior that the hydrate surface exhibits.

The conversion is achieved by adding a cooled hydrocarbon stream containing a large number of dry hydrate particles into the warm oil or condensate well stream containing free water droplets. The water will quickly form a thin water film on the surface of the dry hydrate particles, due to the hydrophilic nature of the hydrate surface. The mixed stream is then cooled further, and the water film is converted to hydrates by growing from the existing hydrate surface and outwards. This prevents agglomeration and deposition later in the process, as there should be no free water encapsulated within the hydrate particles.

The overall objective for the CONWHYP is to achieve:

- Conversion of free water to flow-able dry hydrate particles
- Ending hydrate plugging problems
- Improved hydrate and corrosion control without the use of chemical additives
- Improved environmental performance for offshore hydrocarbon production
- Pipeline transport in thermal equilibrium with the surroundings

This will be realized through the development of a hydrate reactor that is installed close to a wellhead or a pipeline starting point. While the concept is primarily developed with focus on liquid-dominated system, applications to gas-rich systems have also been studied. A schematic of the process is shown in figure 2.25.

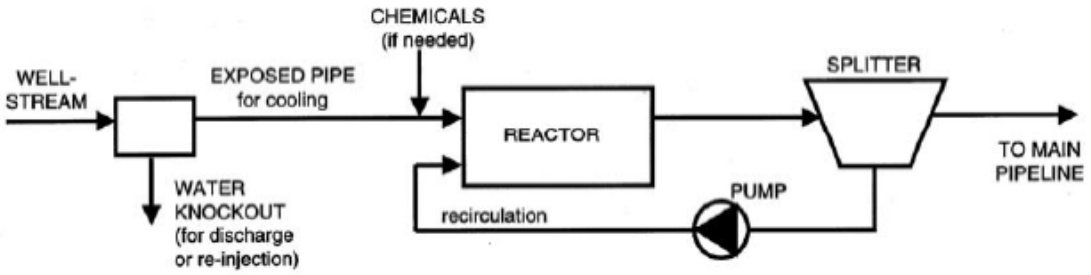

Figure 2.25: Schematic overview of the CONWHYP process (Lund and Larsen, 2000).

At the start of the pipeline, a water knockout drum separates out some of the water, so that no more than a certain amount of water is present in the fluid stream. The stream is then cooled rapidly towards hydrate stability temperatures, through the uninsulated length of pipe. The phases may also be mixed to provide a large interfacial surface area. Following the section of exposed pipe comes the hydrate reactor, where the well stream is mixed with a cold fluid stream coming from a downstream split. In the reactor, free water forms a film around the hydrate particles, and hydrate growth occurs from the existing particle and outwards.

Further cooling takes place through the reactor, and by the time the stream reaches the end of the reactor, it should be fully converted into dry hydrate particles. The splitter downstream the reactor separates out a stream with cold hydrocarbon fluids that is re-injected at the inlet of the reactor.

The second stream from the splitter goes to the main pipeline, and should now consist of only solid, dry hydrate. The aim in the splitting process is that the stream continuing downstream corresponds to the content of water in the inflow to the reactor. The additional cooling in the hydrate reactor will have brought the system

close to ambient temperature, preventing further condensation of water from either liquid or gas hydrocarbon phases for the remainder of the pipeline.

The dry hydrate particles continuing downstream will not melt back to free water and natural gas before it reaches higher temperatures or the pressure becomes too low. This will be at the end of the transportation pipeline, where the process is unproblematic. Sieves can be used to separate the particles from the bulk liquid phase mechanically. In some fluid systems, with the appropriate fluid/particles density, the particles can also be drained from the bottom of the separator tank.

2.5 The Cold Flow Simulator

The flow simulator used in this thesis is sequential modular simulator, implemented in MATLAB. The model is developed by SINTEF as an aid for developing subsea oil and condensate fields by the CONWHYP (Conversion of water to hydrate particles) loop concept.

2.5.1 Model description

The program can simulate any number of fluid streams from subsea wells, templates or fields. The simulator itself is built up of a combination of five different types of units:

- **Sources** (1. and 2.). This unit specifies the mass flow, composition, temperature and thermodynamic properties of the streams.
- **Mixers**
- **Plug flow reactors**. This unit calculated the hydrate conversion and heat exchange with the environment
- **Pipes**. No hydrate conversion is calculated in this unit, but heat transfer to the environment is calculated
- **Splitters**.

All units have one input and one output, except the mixers and splitters. Mixers have two inputs and one output, and splitters have one input and two outputs. Units are numbered 1, 2, 3… N and the streams are given a label corresponding to their upstream unit. As an example, stream A from unit 2 is labeled [2 A].

Figure 2.26 shows an example flowsheet of how the units could be combined in the simulator.

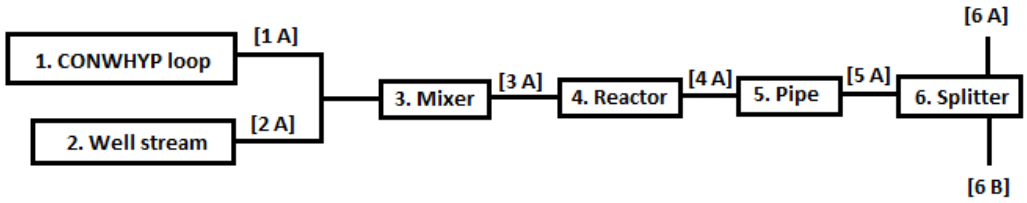

Figure 2.26: Basic flow sheet integrating a well stream (2) to a CONWHYP loop (1)

2.5.2 Model Equations

Thermodynamics and kinetics

Hydrate formation

The process streams are assumed to consist of:

- Hydrate
- Water
- Light Hydrocarbons
- Heavy Hydrocarbons

The composition of the stream is represented by the mass fraction of these four classes. For instance, for a well stream [2 A] consisting of

- No hydrate
- wt. % 8,3 water
- wt. % 13,4 LHC
- wt. % 78,3 HHC

Will have a composition vector [0 0.0083 0.0134 0.0783]. The hydrate formation is assumed to be:

$$x\ kg\ water + y\ kg\ LHC \rightarrow (x+y)\ kg\ hydrate \qquad \textbf{2.7}$$

Enthalpy Calculations

The enthalpy of each of the four composition classes is described by a linear relationship:

$$H_i = \Delta H_{f,i} + C_{p,i}(T - T_{ref}) \qquad \textbf{2.8}$$

where:

- H_i is the enthalpy of composition class i [J/kg]
- $\Delta H_{f,i}$ is the formation enthalpy of class i [J/kg]
- $C_{p,i}$ is the heat capacity of class i [J/kgK]
- T is the temperature [□C]
- T_{ref} is the reference temperature [□C]

Unit models

Mixer

As the mixer has two input streams and one output stream, the mass balance becomes:

$$\dot{m} = \dot{m}_1 + \dot{m}_2 \qquad \textbf{2.9}$$

- $\dot{m}$ is the output mass flow [kg/s]
- $\dot{m}_1$ is the mass flow of input 1 [kg/s]
- $\dot{m}_2$ is the mass flow of input 2 [kg/s]

Two auxiliary quantities are defined as:

$$w_1 = 1 - w_2 = \frac{\dot{m}_1}{\dot{m}_1 + \dot{m}_2} \qquad \textbf{2.10}$$

So that the component mass balance for composition class i is:

$$x_i = w_1 x_{1,i} + w_2 x_{2,i} \qquad \textbf{2.11}$$

Where x_i is the mass fraction of composition class i.

The energy balance may be written:

$$H = w_1 H_1 + w_2 H_2 \qquad \textbf{2.12}$$

We get the following mixing relationships for heat capacity and formation enthalpy:

$$C_p = w_1 C_{p1} + w_2 C_{p2} \qquad \textbf{2.13}$$

$$\Delta H_f = w_1 \Delta H_{f1} + w_2 \Delta H_{f2} \qquad \textbf{2.14}$$

Reactor

A plug flow model is used to describe the reactor. The mass balance for composition class i can be expressed as:

$$\frac{dx_i}{dz} = \frac{A}{\dot{m}} r_i \qquad \textbf{2.15}$$

where:

- A is the cross-sectional area of the reactor [m^2]
- $\dot{m}$ is the mass flow [kg/s]
- r_i is the reaction rate of class i [kg/m^3s]
- x_i is the mass fraction of class i [-]
- z is the axial position in the reactor [m]

The energy balance is expressed as:

$$\frac{dT}{dz} = \frac{-Ua(T - T_\infty - A\sum_i r_i H_i}{\dot{mC}_p} \qquad \textbf{2.16}$$

where:

- Ua is the heat transfer coefficient per meter pipe [W/mK]
- T is the temperature [□C]
- T_∞ is the sea temperature [□C]
- A is the cross-sectional area of the reactor [m^2]
- r_i is the reaction rate of class i [kg/m^3s]
- H_i is the enthalpy of composition class i [J/kg]
- $\dot{m}$ is the mass flow [kg/s]
- C_p is the heat capacity [J/kgK]

Pipe

No reaction is calculated in the pipe unit, only the heat transfer. An auxiliary function is defined by:

$$\gamma(z) = e^{-\frac{Uaz}{\dot{mC}_p}} \qquad \textbf{2.17}$$

and the temperature profile calculated from:

$$T(z) = \gamma(z)T_{in} + \big(1 - \gamma(z)\big)T_{\infty} \qquad \textbf{2.18}$$

where T_{in} is the inlet temperature [□C]

Splitter

As the splitter has one input stream and two output streams, the mass flow outputs are:

$$\dot{m}_1 = \alpha\dot{m} \qquad \textbf{2.19}$$

$$\dot{m}_2 = (\dot{1} - \alpha)\dot{m} \qquad \textbf{2.20}$$

where α is the split factor.

2.5.3 Using the simulator

The first step in putting the simulator to use is to draw a flow sheet of the process, like the one shown in figure 2.26, and numbering all units and streams. The next step is to make an input file. The creator of the simulator has provided a recipe for doing this. The objective of the input file is to set up the following structures:

- **param.** This structure contains constants and parameters, such as heat capacities and names of various files.
- **Item.** This is a cell vector of process units. Each of these process units is described by a structure, containing parameters for the units. A list of entries is given in appendix A.

After the input file is correctly configured, the simulator can be run from the MATLAB command window, and the results are read to an output file.

2.5.4 Modifying the simulator

In order for the MATLAB simulator to be an efficient tool in this thesis, certain modifications have to be made. This includes both what data is present in the output, as well as how they are presented.

In very short terms, the simulator takes in an input file, runs the main script with these inputs, and creates an output file in .txt-format. The input file contains two kinds of structures:

- The **parameters** are where all values needed to perform the calculations are stored. This can either be real values such as the heat capacity of water (param.water), or function handles for when calculations are done in a separate script. For instance, param.viscosity has the function handle @viscosity.
- The **units** contain information about how the system is set up, with the well stream, CONWHYP loop, pipes, reactors and splitters.

Both the parameters and the units in the input-file have to be modified for the intended use of the simulator. The first modifications, however, will be to how the simulator displays output data. As it is currently programmed, the output .txt-file gives a list of all the units, with the relevant parameters listed for each unit. This is a somewhat impractical method of displaying the output data for this papers intended use. It is a tedious task to compare how parameters such as viscosity changes by scrolling through all these units for two different inputs.

To aid in the data interpretation, a new script is created. This script allows for graphical interpretation of the viscosity profile along the flow-line. The script runs the main script for several different input files and stores their viscosity and position values in double vectors by running them through a for-loop. Each of these vectors represent a viscosity profile, all of which are plotted for quick graphical interpretation.

An important benefit of the new script is that we can quickly investigate how the simulator handles changes to specific parameters in the input data. We can easily set up several identical input files, and then change one parameter in the input files to examine the effect. The results give an indication of whether or not the simulator behaves correctly according to rheology theory, and we can begin modifying the simulator based on these results.

To illustrate how this support script is used, we will start with two identical input files. Running the script results in a plot of the viscosity profile (viscosity vs. position). As expected, the two profiles are identical (figure 2.27), but it gives confirmation that the input files have the same set up, and that any change to the profiles can be credited to the specific parameter we choose to change.

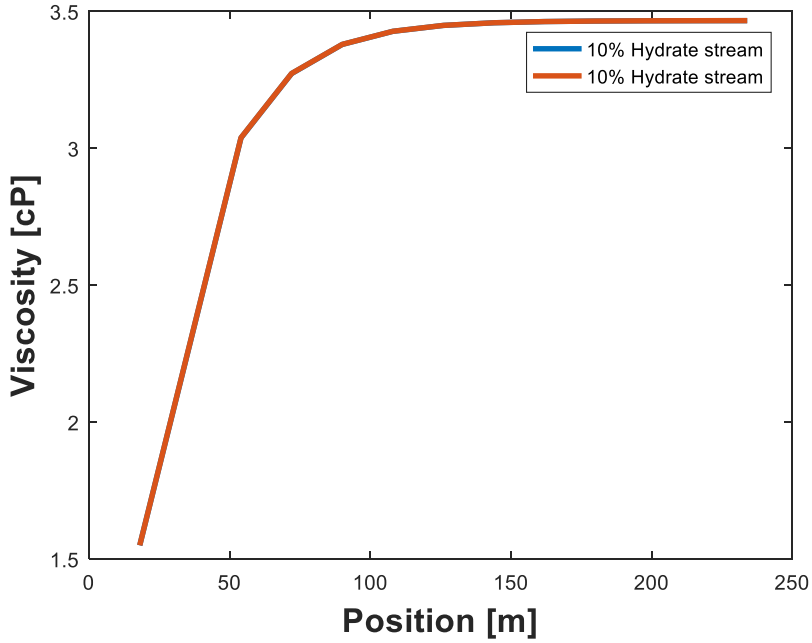

Figure 2.27: Two overlapping viscosity curves as a result of identical input data

Next, the same input files are used, but with different values for the "hydrate particle diameter". All other parameters, such as composition, heat capacities and temperatures are the same.

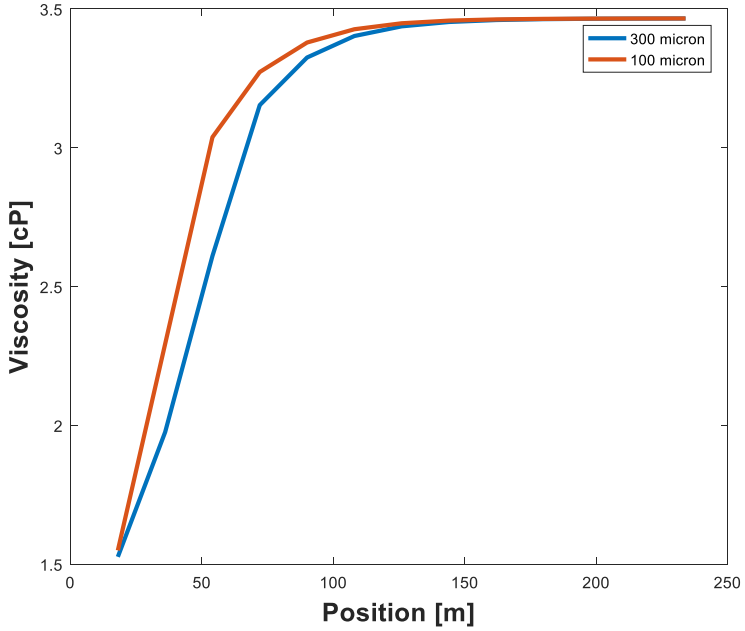

Figure 2.28: Viscosity profile for two stream with different hydrate particle diameter

With different size hydrate particles, it can be seen from the graph in figure 2.28 that the viscosity profile also changes. The system experiences a higher viscosity for the case with smaller size particles. At first glance, this observation is in agreement with the theory on effect of particle size explained in chapter Rheology Theory. However, we see from the graph that the two viscosities eventually end up on the same values, which would not be the case if we have two identical systems with only the particle size being different. It is therefore reasonable to attribute the difference in viscosity to something else.

Looking through the output values in each unit step by step reveals that the reason we get different viscosities is the way the simulator calculates reaction rate. For smaller particles, who will have a larger surface area for the same total volume of hydrate, will have a higher reaction rate than the bigger particles. Thus, the reaction is faster, and for a given time, more hydrate has been created. This leads to an increase in viscosity. Once the system with larger particles has completed the conversion, the viscosities are equal. Because the reaction itself is of no interest when looking strictly on rheology effects, this unwanted result is countered by setting the hydrate reaction rate to zero. This way, no hydrate is converted, and the reaction rate no longer influences the viscosity of the system.

2.5.4.1 The viscosity function

The apparent viscosity of the system simulated is calculated in the script named viscosity.m using the following equation:

$$\mu_a = 10^{A+\frac{B}{T}} * e^{weight\ frac\ coefficient*100*x(1)} \quad \textbf{2.21}$$

The first term in the equation expresses how a Newtonian fluid's viscosity varies with temperature. The viscosity of all simple liquids decreases with increase in temperature because of the increasing Brownian motion of their constituent molecules, and generally the higher the viscosity, the greater the rate of decrease (Barnes, 2000). The expression used here is the most widely-used, credited to E.N. Andrade:

$$\log_{10}\mu = A + \frac{B}{T} \qquad \textbf{2.22}$$

Where T is the temperature in Kelvin. The coefficients A and B are calculated as:

$$B = \left(\frac{T_0 T_1}{T_0 - T_1}\right)\log_{10}\frac{\eta_1}{\eta_0} \qquad \textbf{2.23}$$

And

$$A = \log_{10}\eta_0 - B/T_0 \qquad \textbf{2.24}$$

Where:

- T_0 is the temperature at low viscosity [K]
- T_1 is the temperature at high viscosity [K]
- μ_0 is the assumed viscosity at T_0
- μ_1 is the assumed viscosity at T_1

Because this expression is independent of the parameters we want to investigate, it will stay unaltered in the modified version of the viscosity calculation.

Following the expression for thermal variation, we have the exponential expression that accounts for the hydrate phase volume present. This expression has been derived through empirical methods. The expression is based on the Kreiger-Dougherty equation, where parameters such as the maximum packing fraction has been fitted to the curve through laboratory experiments. Because of confidentiality, it is difficult to explain the model to more detail. That being said, since this model is developed based on laboratory test for the actual oil in question, it does represent the most accurate estimate of how the viscosity changes.

The exponential expression is replaced by the conventional K-D equation, giving us the following expression for the hydrate slurry viscosity:

$$\mu_a = 10^{A+\frac{B}{T}}\left(1 - \frac{x_{hydrate}}{\phi_m}\right)^{-[\eta]\phi_m} \qquad \textbf{2.25}$$

Where μ is the continuous phase viscosity and $[\eta]$ is the intrinsic viscosity. As stated in the chapter about rheology theory, the product of the intrinsic viscosity and maximum packing fraction almost always takes a value close to 2. This simplification reduces the equation to:

$$\mu_a = 10^{A+\frac{B}{T}}\left(1-\frac{x_{hydrate}}{\phi_m}\right)^{-2}$$

3 Simulation results and discussion

As the viscosity function is now properly modified, simulations can be made to investigate how different parameters affect the viscosity of the system. Simulations will be done by separately altering specific parameters in the input data, with focus on parameters that according to rheology theory are significant. In each section, the viscosity profile and pressure gradient of the simulated system are presented and discussed. The four parameters that will be evaluated are:

- **Hydrate volume fraction (HVF).** This will be done by changing the composition of the well stream containing hydrates.
- **Particle size distribution (PSD).** The degree of polydispersity directly affects the maximum packing fraction ϕ_m. A polydisperse population with a broad size distribution packs more closely than a monodisperse sample, yielding a higher maximum packing fraction (MPF). According to literature (Fletcher, 2017), a monodisperse sample has a maximum packing fraction of around 62%. In a polydisperse sample, where smaller particles can fill gaps between larger particles, the maximum packing fraction is around 74%. Consequently, this is the range that will be used in the simulation.
- **Water cut.** As with hydrate volume fraction, the effect of changes in the water cut will be simulated by changing the composition of the system. This simulation will also include the formation of hydrates through the pipeline
- **Particle size.** Based on rheology theory in relation to hydrate particle size, it is not expected to experience any significant viscosity effects due to changes in this parameter. However, the particle size may influence other parameters connected to the pressure drop.

This chapter will present and discuss these results. The complete input/out files and relevant scripts can be found in the appendix section.

3.1 Hydrate volume fraction

The impact of hydrate volume fraction on the viscosity will be investigated by running the simulation for four different compositions. The hydrate volume fraction will range from 5% to 40%, as seen in table 3:

	Volume fractions [%]			
	Case 1	Case 2	Case 3	Case 4
Component				
Hydrate	5	15	30	40
Water	4,15	4,15	4,15	4,15
Light HC	12,7	12,7	12,7	12,7
Heavy HC	78,15	68,15	53,15	43,15

Table 3: Fluid compositions for HVF simulations

All input parameters beside the composition is kept identical. In figure 3.1, the viscosity profile of each case is presented:

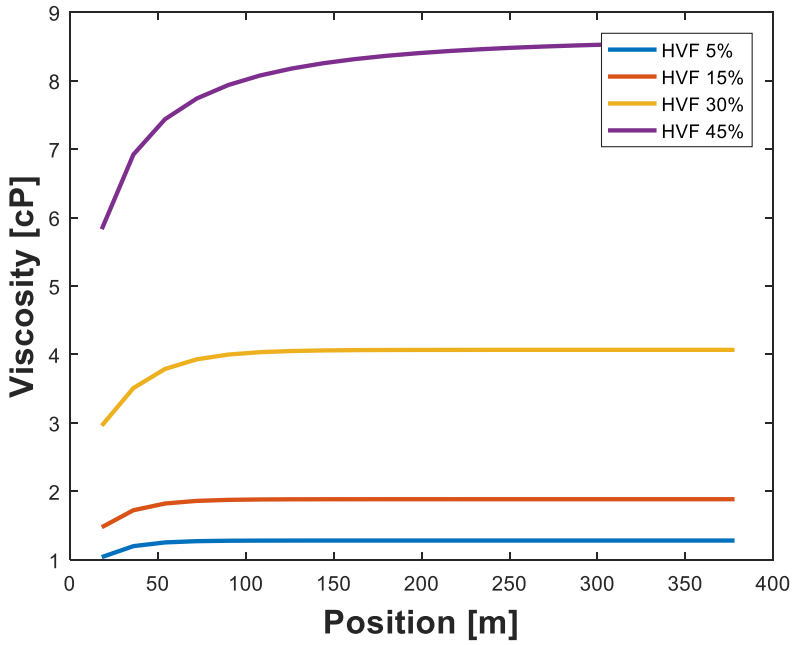

Figure 3.1: Viscosity profile for a range of hydrate volume fractions

HVF [%]	Viscosity [cP]	Relative increase [%]
40	8,56	567,91
30	4,07	217,29
15	1,89	47,08
5	1,28	0,00

Table 4: Steady state viscosities for the different HVF

It can be seen from the graph and table 4 that, depending on the hydrate volume fraction, we get a significantly different viscosity profile. It indicates that by going from 30% to 45% hydrate in the system, the viscosity will more than double. In other words, the amount of hydrates present in the stream will have great impact on the systems deliverability. Figure 3.2 shows the pressure profiles for the respective viscosity profiles:

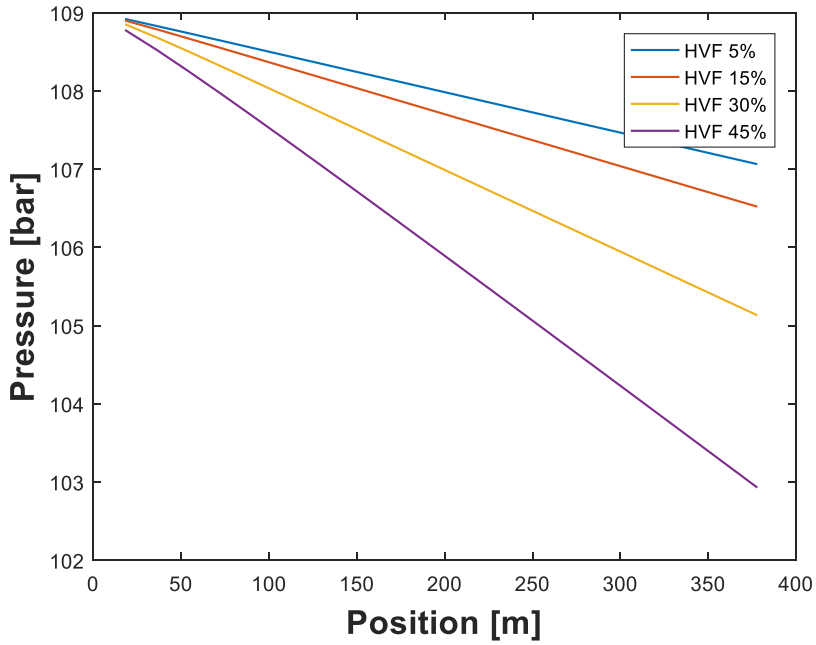

Figure 3.2: Pressure profiles at the four different HVFs

HVF [%]	Pressure [bar]	Deviation [%]	Pressure gradient [bar/100m]
40	102,93	3,86	1,61
30	105,13	1,80	1,02
15	106,52	0,51	0,66
5	107,06	0,00	0,51

Table 5: Pipeline pressures at 378m for different HVFs

As a consequence of the big difference in viscosities, we also get very different pressure profiles. Not surprisingly, the greatest pressure drop occurs in the

system with the highest viscosity. It can be seen from table 5 that, over the length of 378m pipe, the pressure drops around 4 bar more for the 40% HVF case compared to 5% HVF. Such a dramatic pressure gradient would inarguably be unfeasible for hydrocarbon transportation over longer distances.

The simulations run show that the hydrate volume fraction is undoubtedly a significant parameter when looking at the pressure profile in a pipeline. However, it is not an independent variable, and the significance will vary with the maximum packing fraction of the system, as will be shown in the following section.

3.2 Particle size distribution

3.2.1 10% Hydrate volume fraction

In this simulation the composition is set to an arbitrary value for the hydrate volume fraction, since the focus is how the viscosity varies with the *maximum packing fraction.* The following compositions are used in the input:

	Volume fractions [%]		
	Hydrate stream	Well stream	Mixed
Hydrate	20	0	10
Water	0	8,3	4,15
Light HC	12	13,4	12,7
Heavy HC	68	78,3	73,15

Table 6: Fluid composition in PSD simulation for 10% hydrate fraction

Figure 3.3 shows the hydrate slurry viscosity in a 378m pipeline. As the system reaches steady state, the viscosity takes four different values depending on the MPF. The viscosity is calculated to 1.46 cP for the fully polydisperse distribution, and gradually increases with decreasing polydispersity up to 1.56 cP for the monodisperse sample. This result is in agreement with the rheology theory presented in section 2.3.6, which states that a sample of more randomly sized particles will have a lower viscosity than a system with uniform particle size.

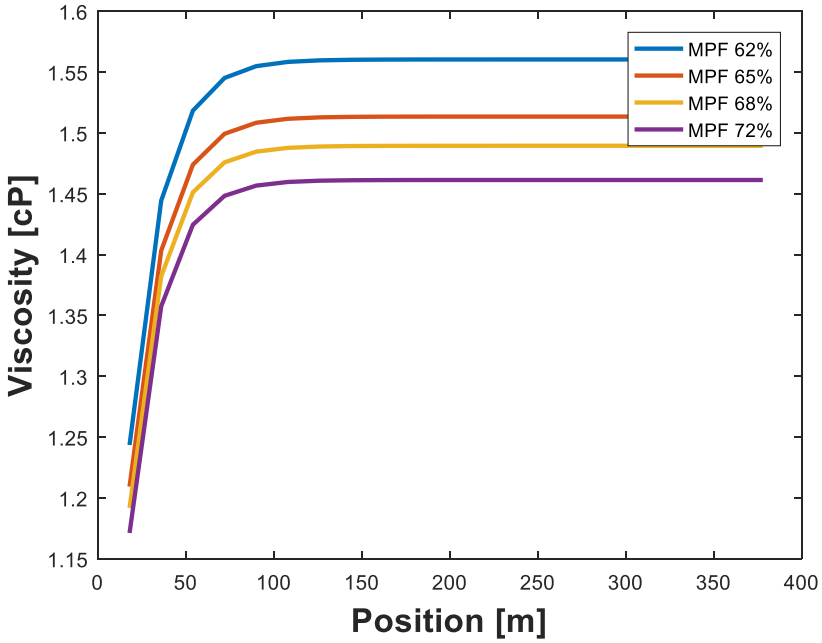

Figure 3.3: Viscosity in a pipeline for a range of maximum packing fractions

MPF [%]	Steady state viscosity [cP]	Relative increase [%]
62	1,56	6,78
65	1,51	3,57
68	1,49	1,92
72	1,46	0,00

Table 7: Steady state viscosities and relative increases at the different MPFs

The increase in viscosity from the highest to the lowest MPF is only 0.1 cP, or around 7%. However, over a long pipeline, this difference may be significant to the pressure drop. In figure 3.4 the pressure profile of the pipeline is presented:

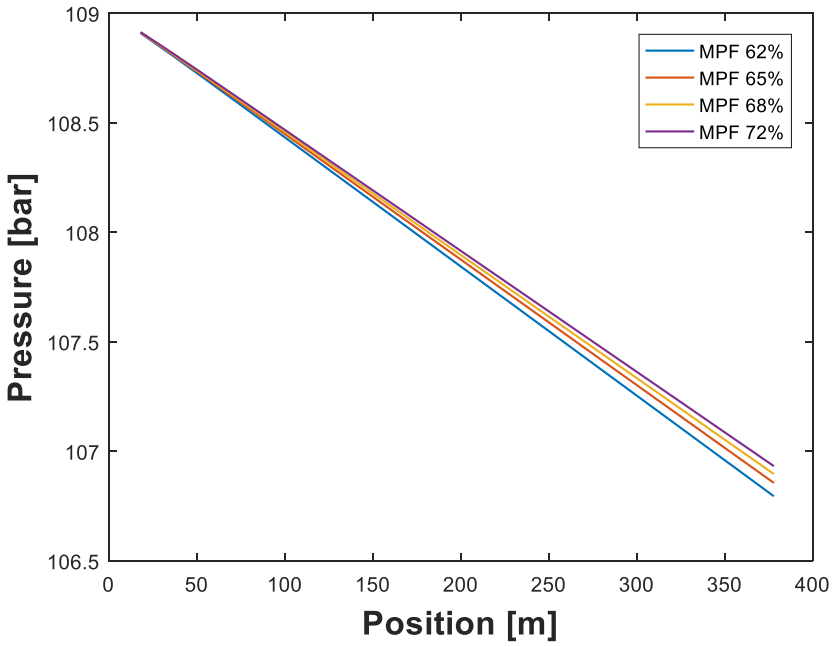

Figure 3.4: Pressure profile in the pipeline.

As expected, the different viscosities will result in four different pressure profiles, with the polydisperse system generating the lowest pressure drop. The four pressures at 378m are presented in table 8.

MPF [%]	Pressure [bar]	Deviation [%]
62	106,80	0,12
65	106,86	0,07
68	106,90	0,03
72	106,93	0,00

Table 8: Pressures at 378m

Only 0.13 bar, or 0.12%, separate the two extreme MPFs, indicating that the maximum packing fraction may not be a significant parameter when looking at pressure drops in a pipeline. Even for a long pipeline of 4000m, the outlet pressures would only differ with 1.3 bar. However, this parameter has to be evaluated in relation to the hydrate volume fraction. Higher hydrate volume fractions than 10% may change the importance of the MPF. This will be investigated in the next section.

3.2.2 30% Hydrate volume fraction

As in 3.2.1, the impact of the MPF will be investigated, but now with a higher fraction of hydrate present in the stream. The following compositions are used in the input:

	Volume fractions [%]		
	Hydrate stream	Well stream	Mixed
Hydrate	60	0	30
Water	0	8,3	4,15
Light HC	12	13,4	12,7
Heavy HC	28	78,3	53,15

Table 9: Fluid composition in PSD simulation for 30% hydrate fraction

With the new compositions, the viscosity profiles are simulated with the same MPFs. Results are presented in figure 3.5:

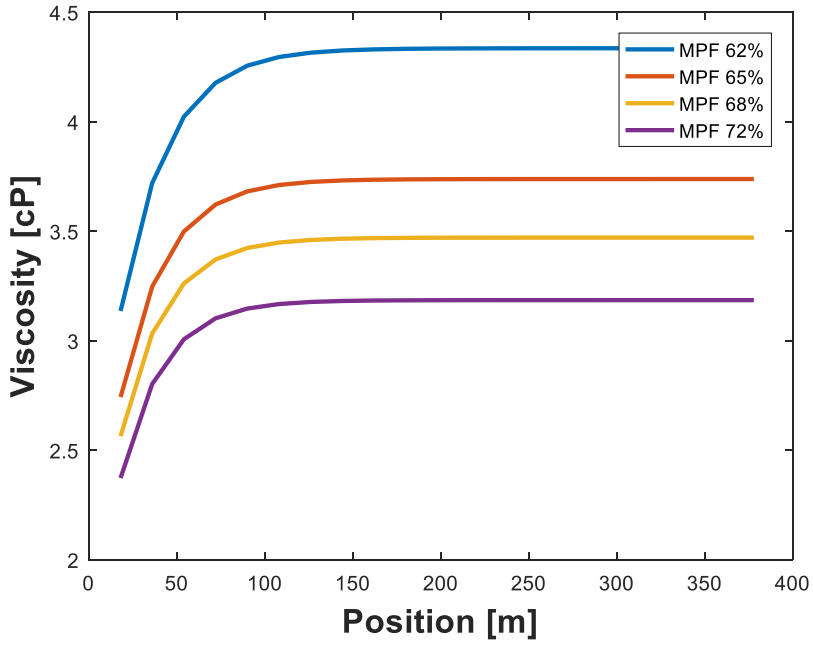

Figure 3.5: Viscosity vs. position in the pipeline at different MPFs

As in the case with a hydrate volume fraction of 10%, the trend is that a lower MPF yields a higher viscosity. With 30% hydrate volume fraction, however, we get a higher viscosity, and the relative increase is bigger than in the previous simulation. The steady state viscosities and relative increases are presented in table 10:

MPF [%]	Viscosity [cP]	Relative increase [%]
62	4,33	36,11
65	3,74	17,36
68	3,47	8,96
72	3,18	0,00

Table 10: Steady state viscosities and relative increases for the different MPFs

With a higher HVF, the viscosity of the monodisperse sample is around 36% higher than the fully polydisperse sample. This difference in viscosity may be significant when evaluating the pressure drop along a pipeline. Figure 3.6 shows the pressure profile for a 378m pipe under these conditions:

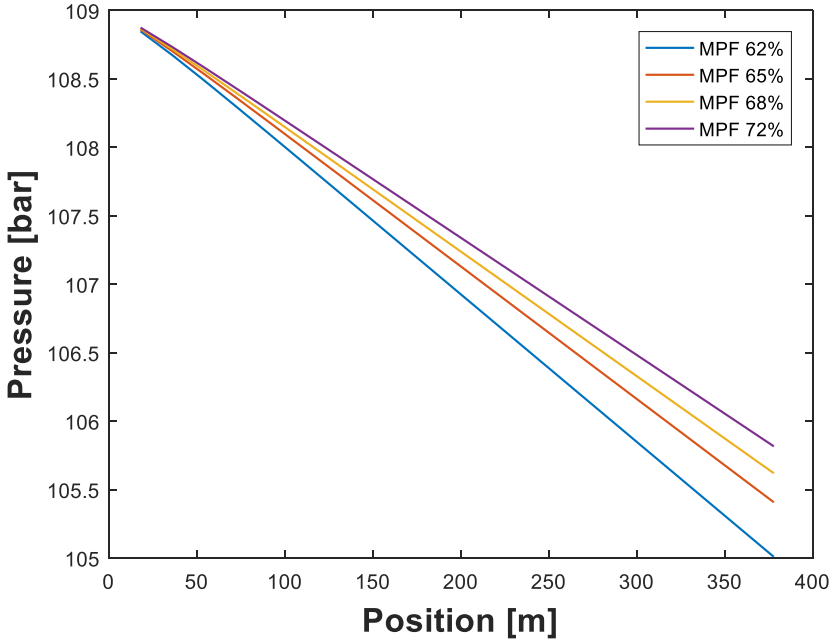

Figure 3.6: Pressure profile for 30% hydrate volume fraction.

MPF [%]	Pressure [bar]	Deviation [%]	Pressure gradient [bar/100m]
62	105,01	0,77	1,06
65	105,41	0,39	0,95
68	105,62	0,19	0,89
72	105,82	0,00	0,84

Table 11: Pressures at 384m and pressure gradients for 30% HVF

From table 11 it can be seen that the pressure gradients for the two extreme MPFs now deviate by around 0.2 bar. While still a small deviation, this may prove to be significant for long pipelines. For instance, for a 4000m pipeline, the pressure

difference would be 8 bar, solely because of the difference in particle size distribution. Hence, manipulation of the maximum packing fraction could under the right circumstances prove to be a useful tool when considering means to improve flow system deliverability.

3.3 Particle Size

As in the previous sections, four simulation are run to investigate the impact of particle size. Four different sizes will be spanning from 10 μm to 150 μm. This range is taken from research by Sun et al., who measured hydrate particle size using a focused beam reflectance measurement probe (Sun et al., 2015). The purpose of using this range is to use particle sizes that one may expect to encounter in a real situation.

Figure 3.7 shows the viscosity profile for the four different cases, where in all cases the HVF and MPF are 30% and 62%, respectively:

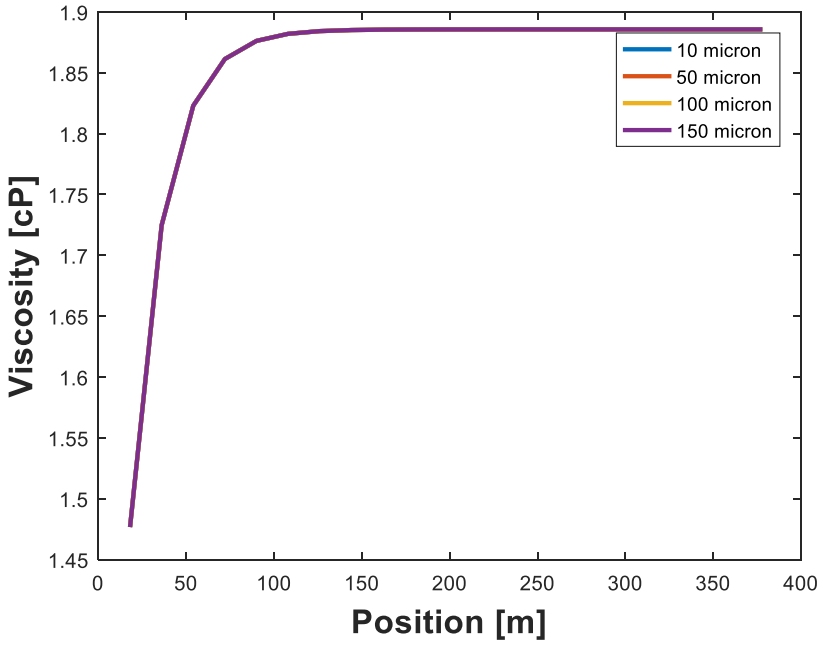

Figure 3.7: Four overlapping viscosity profiles at the different hydrate particle sizes

As expected, the four curves overlap, since the hydrate particle diameter is not a parameter in the viscosity calculation. As stated in section 2.3.9, for particles smaller than 10 μm, the van-der-Waals interaction potential is not significant, and is therefore not included in the viscosity calculation.

While the hydrate particle size may not influence the viscosity, the pressure profile of the system may change. Figure 3.8 shows the pressure profiles of the four cases:

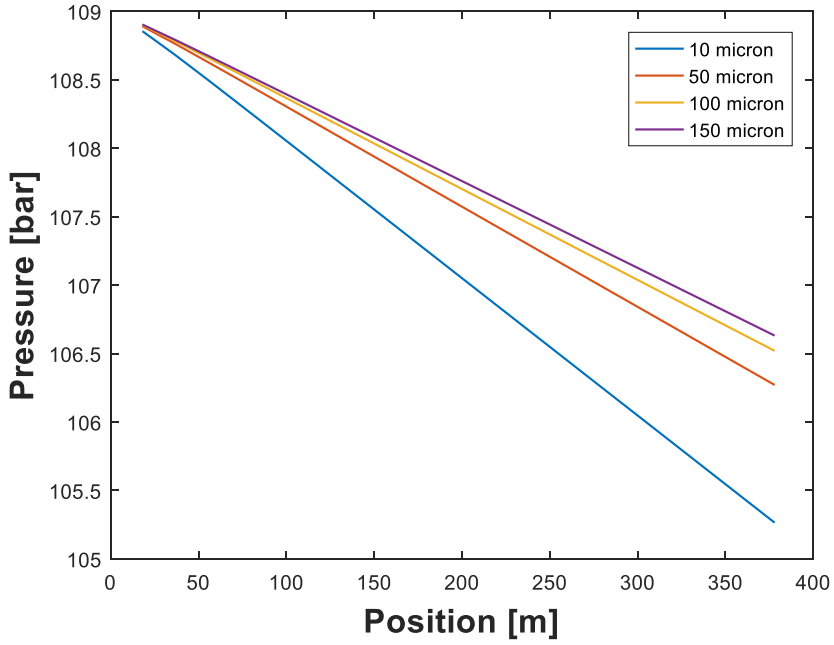

Figure 3.8: Pressure profiles for the different hydrate particle sizes

Dpart [micron]	Pressure [bar]	Deviation [%]	Pressure gradient [bar/100m]
150	106,63	1,30	0,63
100	106,52	1,19	0,66
50	106,27	0,96	0,72
10	105,26	0,00	0,99

Table 12: Pressures at 378m and pressure gradients for the four cases

As can be seen in the plot and table 12, the pressure gradients vary significantly. This is because the pressure drop calculation in the simulator is a function of the slurry friction factor, which again is a function of the hydrate particle size. More specifically, the drag coefficient used in the friction factor calculation is a function of the particle size. The scripts handling the slurry friction factor and drag coefficient can be found in the appendix.

The system with hydrate particles of size 10 μm exhibits a pressure gradient of approximately 1 bar, whereas the system with 150 μm-sized particles have a pressure gradient of around 0.6 bar. Again, such a difference would yield a significant drop in pressure over longer distances, and indicates that a system with large hydrate particles is preferred. However, this may not be the case when evaluating a hydrate system. In pipelines, hydrate particles stick to each other by capillary forces. These aggregates trap free liquid and gas, which results in an effective volume fraction much higher than the true hydrate volume fraction because of liquid entrapment. We have seen in

section 3.1 that a hydrate slurry system is highly sensitive to changes in the hydrate volume fraction. AAs reduce the capillary forces, leading to a decrease in the effective hydrate volume fraction, resulting in slurry flow without plugging. Research efforts have therefore been made to develop AAs that decrease the size of hydrate particles, rather than increasing them (Sun et al., 2016).

3.4 Water cut

Impact of changes to the water cut will be investigated in the familiar way of simulating four nearly identical systems, with the only difference being the water volume fraction. The four compositions that will be simulated are given in table 13:

	Volume fractions [%]			
	Case 1	**Case 2**	**Case 3**	**Case 4**
Component				
Hydrate	15	15	15	15
Water	5	15	25	35
Light HC	11	11	11	11
Heavy HC	69	59	49	39

Table 13: Initial compositions of the four simulations with different water cuts

While the simulations of the water cut impact is done by the seemingly same method as the simulations in the previous section, there is one important difference. Previous simulations were investigations of the flow based strictly on rheology theory, with a fixed volume fraction of hydrate throughout the length of the pipeline. When the impact of the water cut is evaluated, it will be done in a system where actual formation of new hydrates occurs. In this case, the hydrate reaction rate function that was earlier deactivated is therefore activated again.

Figure 3.9 shows how the viscosity now develops throughout a pipeline for the four different cases:

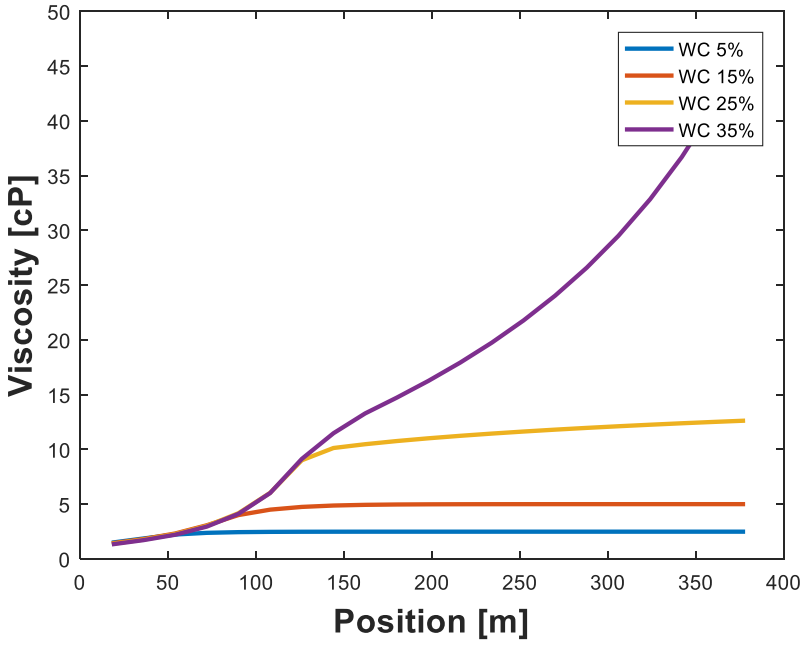

Figure 3.9: Viscosity profiles for the four cases with different initial water cuts

The figure shows how we get significantly different viscosity profiles depending on the initial water cut of the system. This difference can be attributed to the role water plays in the formation of hydrates. As mentioned in section 2.1.2, one of the requirements for hydrate formation is the presence of water. Consequently, more hydrates are allowed to form in a system where more water is present, and the formation will be limited by the availability of water. This is a direct consequence of the behavior of the four viscosity curves in figure 3.9, where it can be seen that the viscosity increases rather rapidly early in the pipeline, but slows down as the water is consumed and transformed into hydrates. The cases where more water is present are allowed to keep forming hydrates for a longer time, and therefore return a higher viscosity.

Reviewing the results from section 3.1, where the impact of hydrate volume fraction was investigated, it is clear that the same mechanisms are in play in this simulation. Figure 3.10 shows how the hydrate volume fraction changes through the pipeline:

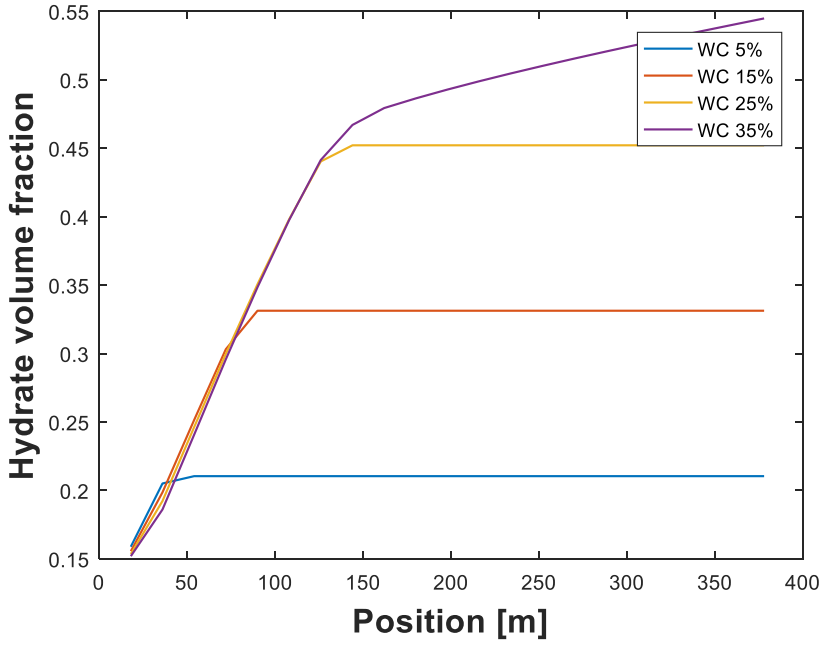

Figure 3.10: Hydrate volume fraction in the pipeline for four different water cut cases

Comparing figure 3.10 to figure 3.9 shows the connection between how the viscosity increases to how the hydrate volume fraction increases in the system. The rapid growth in viscosity ceases as soon as no more hydrate is formed, yielding a more or less steady state viscosity.

The simulation results show how systems with high water cuts will experience great increases in viscosity. These results are in agreement with the studies made on rheology theory, and the limitations of anti-agglomerants reviewed in chapter 2.2.3.

3.5 Sensitivity analysis

The simulations done when investigating the hydrate volume fraction and maximum packing fraction reveals that the relationship between these two variables is just as interesting as merely investigating them separately. It has been shown how the viscosity increases with the hydrate volume fraction and how the viscosity decreases with lower maximum packing fractions. However, these variations are strongly dependent on the other variable. This relationship has motivated to perform a simple sensitivity analysis on the two variables.

The sensitivity analysis is performed by creating a new MATLAB script (Appendix J) that evaluates the viscosity for a range of HVFs and MPFs by running

them through a double for loop. The results are then illustrated by a surface plot. The analysis returns the following data table:

		HVF							
		5 %	**10 %**	**15 %**	**20 %**	**25 %**	**30 %**	**35 %**	**40 %**
MPF	**62 %**	1,18	1,42	1,74	2,18	2,81	3,75	5,27	7,94
	64 %	1,18	1,40	1,71	2,12	2,69	3,54	4,87	7,11
	66 %	1,17	1,39	1,67	2,06	2,59	3,36	4,53	6,44
	68 %	1,17	1,37	1,65	2,01	2,50	3,20	4,25	5,90
	70 %	1,16	1,36	1,62	1,96	2,42	3,06	4,00	5,44
	72 %	1,15	1,35	1,60	1,92	2,35	2,94	3,79	5,06

Table 14: Data table from sensitivity analysis of the variables HVF and MPF

The same trend that was observed in the simulations is evident. The viscosity at a low MPF is more sensitive to a change in HVF compared to the viscosity at a high MPF. Analogously, viscosity at a low HVF is not as sensitive to a change in MPF as a viscosity at a high HVF. Figure 3.11 shows these results graphically:

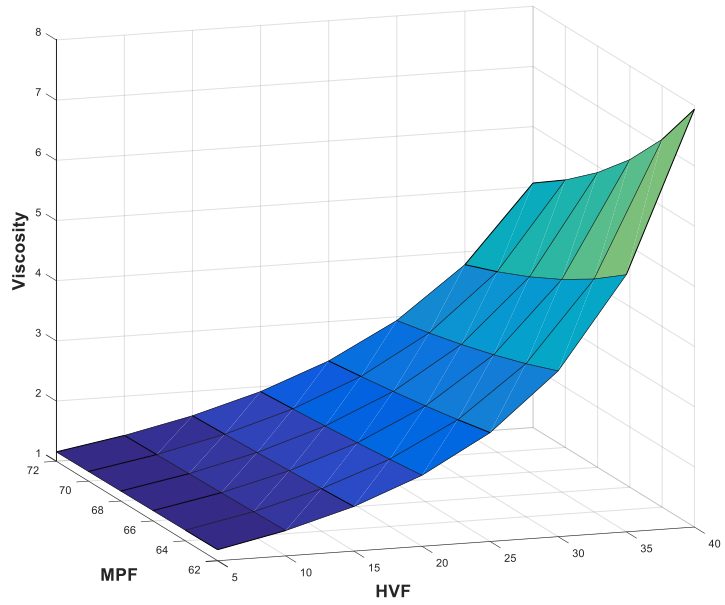

Figure 3.11: Surface plot of MPF vs HVF vs Viscosity

4 Conclusion and further work

Rheology is a beast with many heads. Developing a rheology model that is valid for any given system is close to impossible considering the broad range of behavior a flowing suspension can exhibit, such as differences in viscoelastic/plastic and thixotropic effects. The best method of determining the rheology of a system will therefore always be to fit the rheology curve to measured experimental data, as is done in the simulator used in this thesis. To investigate the impact of specific parameters in the rheology model, the original viscosity expression was replaced by the conventional Kreiger-Dougherty equation. This modification is likely to have made the viscosity calculation less accurate for this specific system, but allowed for a qualitative evaluation of the viscosity profile, based on concepts in fundamental rheology theory. The simulations performed have shown that the system behaves as expected when these concepts were applied. It has also been shown how sensitive the viscosity of the system is to changes to the parameters in question.

Evaluating the hydrate volume fraction and maximum packing fraction revealed that the interplay between these two parameters dictates the impact on the calculated viscosity. These results are important in an event where one might want to manipulate the system to achieve enhanced pipeline performance through viscosity reduction. For instance, we have seen through the simulations that a higher MPF is favorable due to lower viscosity and lower pressure drop. A higher MPF could be achieved by altering the particle size distribution of the system towards higher polydispersity. However, the simulation results also showed that the impact of change in MPF is only significant for higher hydrate volume fractions.

Simulations run with different water cuts showed how the system viscosity increases through the pipeline based on the initial water volume fraction. In this simulation, the system was configured to form hydrates in the heat reactor modules. This resulted in a steadily increasing hydrate volume fraction along the pipeline, thus yielding an increasing viscosity. The viscosity increased rapidly until there was no longer any water present to form hydrates. These results are essentially due to the same mechanisms that was seen in the simulations made on different hydrate volume fractions, but gives a better picture of how the increase in viscosity due to increasing hydrate volume fraction occurs in practice. These results corroborate theory on anti-

agglomerants, which states that one of its limitations is dramatic viscosity increases on higher water cuts.

Effects of hydrate particle size were simulated with four different particle diameters. One assumption made when configuring the simulator was that hydrate particles are too big to experience differences in van-der-Waals interaction potential based on their size. Thus, the simulation yielded identical viscosity profiles for the four cases. However, the hydrate particle size does have impact on the system. Plotting the pressure profile revealed that smaller particles resulted in a significantly higher pressure gradient than bigger particles. This would indicate that bigger particles are favourable. While that may be the case for many suspensions, it is not for hydrates. Taking into consideration how hydrates are formed, with encapsulation of gas and water between particles, bigger hydrate particles will result in a higher effective hydrate volume fraction. As we have seen in the simulations made on the HVF, the system viscosity and pressure profile are highly sensitive to changes in the HVF. Hence, any efforts to optimize system deliverability by altering particle size should therefore put in decreasing the size of the hydrate particles.

For further examination of the rheology of a hydrate suspension, the most interesting subject to investigate next would be the shear-thinning behavior that natural gas hydrates have been known to exhibit. Shear-thinning means that the viscosity decreases at higher shear rates/velocities. All simulations made in this thesis have been on a constant velocity, thereby ignoring this phenomenon. This behavior could be simulated by changing the flow rate or pipe diameter, and the implementing a new rheological model, such as Bingham, Power Law or Herschel-Bulkley, who all describe the shear-thinning phenomenon.

5 Definitions and Nomenclature

5.1 Abbreviations

AA	Anti-Agglomerant
CAPEX	Capital Expenditure
CONWHYP	Conversion of water to hydrate particles
HHC	Heavy Hydrocarbon
HVF	Hydrate Volume Fraction
K-D	Kreiger-Dougherty
KHI	Kinetic Inhibitor
LDHI	Low Dosage Hydrate Inhibitor
LHC	Light Hydrocarbon
MEG	Mono-Ethylene Glycol
MeOH	Methanol
MPF	Maximum Packing Fraction
OCNS	Offshore Chemical Notification Scheme
P&T	Pressure and Temperature
PSD	Particle Size Distribution
QAS	Quaternary Ammonium Surfactants
THI	Thermodynamic Inhibitor
WC	Water cut

5.2 Nomenclature and symbols

sI	Structure I gas hydrate
wt. %	Weight percent
$\boldsymbol{\eta}$	Viscosity
$\boldsymbol{\eta_0}$	Viscosity of the Newtonian continuous phase
$\boldsymbol{\phi}$	Phase volume
$[\boldsymbol{\eta}]$	Intrinsic viscosity
$\boldsymbol{\epsilon}$	Relative permittivity of the continuous phase
$\boldsymbol{\zeta}$	Electrokinetic potential
$\boldsymbol{\sigma}$	Specific conductivity of the continuous phase
$\boldsymbol{a}$	Radius of the spherical particles
$\boldsymbol{\phi_m}$	Maximum packing fraction
$\boldsymbol{H_i}$	Enthalpy of composition class i
$\Delta\boldsymbol{H_{f,i}}$	Formation enthalpy of class i
$\boldsymbol{C_{p,i}}$	Heat capacity of class i
$\boldsymbol{T}$	Temperature
$\boldsymbol{T_{ref}}$	Reference temperature
$\dot{\boldsymbol{m}}$	Output mass flow
$\dot{\boldsymbol{m}}_1$	Mass flow of input 1
$\dot{\boldsymbol{m}}_2$	Mass flow of input 2
$\boldsymbol{w_i}$	Weight fraction
$\boldsymbol{x_{j,i}}$	Mass fraction for component j of class i
$\boldsymbol{A}$	Cross-sectional area of the reactor
$\boldsymbol{r_i}$	Reaction rate of class i
$\boldsymbol{z}$	Axial position in the reactor
$\boldsymbol{Ua}$	Heat transfer coefficient
$\boldsymbol{\gamma}$	Auxiliary function for temperature profile calculation
$\boldsymbol{T_{in}}$	Inlet temperature
$\boldsymbol{\alpha}$	Split factor
$\boldsymbol{A/B}$	Coefficients for viscosity calculation
$\boldsymbol{x\_hydrate}$	Hydrate volume fraction

6 List of Equations

7 Bibliography

Giavarini and Hester, 2011: Giavarini, Hester, Gas Hydrates – Immense Energy Potential and Environmental Challenges, Springer-Verlag London Limited

Max et al, 2006: M.D. Max, A.H. Johnson, W.P. Dillon, Economical geology of natural gas hydrates, Springer, Dordrecht

Todd et al., 1996: J.L. Todd et al., Reliabilty Engineering—Gas Freezing and Hydrates, Texaco Company Hydrate Handbook, New Orleans, LA

Palermo and Sloan, 2011: Palermo, E.D. Sloan, et al., Natural Gas Hydrates in Flow Assurance, Elsevier Inc.

Sloan, 2000: E.D Sloan, Hydrate Engineering. In: SPE Monograph, vol. 21. Society of Petroleum Engineers, Inc., Richardson, Texas

Kelland, 2009: M.A. Kelland, Production Chemicals for the Oil and Gas Industry, CRC press Taylor and Francis Group, London, UK

Frostman, 2000: L. M. Frostman, Anti-agglomerant hydrate inhibitors for prevention of hydrate plugs in deepwater systems, SPE Annual Technical Conference and Exhibition, Society of Petroleum Engineers, Dallas, Texas, US

Phillips and Grainger, 1998: N. J. Phillips, M. Grainger, Development and Application of Kinetic Hydrate Inhibitors in the North Sea, SPE 40030 (paper presented at the Proceedings of the Annual Gas Technology Symposium, Society of Petroleum Engineers, Calgary, Alberta, Canada

Rojey et al., 1998: A. Rojey, M. Thomas, A. Delion, J. Durand, Process for transporting a fluid such as dry gas likely to form hydrates, Institut Francais Du Petrole, Patent US5816280A

Erstad et al., 2008: K. Erstad, S. Hoeiland, T. Barth, P. Fotland, Isolation and Molecular Identification of Hydrate Surface Active Components in Petroleum Acid Fractions, Proceedings of the 6th International Conference on Gas Hydrates (ICGH 2008), Vancouver, British Columbia, Canada

Hemmingsen et al., 2006: P. Hemmingsen, X. Li, J. Peytavy, J. Sjöblom, Hydrate Plugging Potential of Original and Modified Crude Oils, The Ugelstad Laboratory, Department of Chemical Engineering, NTNU, Trondheim, Norway

Bergfløt, 2001: L. Bergfløt, Influence of Crude Oil Based Surface Active Components and Synthetic Surfactants on Gas Hydrate Behaviour, PhD thesis, University of Bergen, Norway

Høiland et al., 2005: S. Høiland, A. E. Alagic, T. Barth, P. Fotland, K. Askvik, F. Fadnes, Wettability of freon hydrates in crude oil/brine emulsions, Department of Chemistry, University of Bergen, Bergen, Norway

Palermo et al., 2004: T. Palermo, A. Mussumeci, E. Leporcher, Could Hydrate Plugging Be Avoided Because of Surfactant Properties of the Crude Oil and Appropriate Flow Conditions?, Offshore Technology Conference, Houston, Texas, U.S.

Mehta et al., 2003: A. P. Mehta, P. B. Herbert, E. R. Cadena and J. P. Weatherman, Fulfilling the Promise of Low-Dosage Hydrate Inhibitors: Journey From Academic Curiosity to Successful Field Implementation, SPE 81927, Publication from paper OTC 14057, prepared for presentation at the 2002 Offshore Technology Conference, Society of Petroleum Engineers, Houston, Texas, US

Kelland et al., 1995: M.A. Kelland, T. M. Svartaas, L. Dypvik, Studies on New Gas Hydrate Inhibitors, SPE 30420, Prepared for presentation at the SPE Offshore Europe Conference, Society of Petroleum Engineers, Aberdeen, Scotland

Fu et al., 2001: S. B. Fu, L. M. Cenegy and C. S. Neff, A Summary of Successful Field Applications of A Kinetic Hydrate Inhibitor, SPE 65022, Presented at the 2001 SPE International Symposium on Oilfield Chemistry, Society of Petroleum Engineers, Houston, Texas, US

Shi et al., 2015: Bo-Hui Shi, Shuai Chai, Lin-Yan Wang, Xiaofang Lv, Hui-Shu Liu, Hai-Hao Wu, Wei Wang, Da Yu, Jing Gong, Viscosity investigation of natural gas hydrate slurries with anti-agglomerants additives, Fuel 185, Elsevier Ltd

Wagner, 1891: Wagner, J., Zeit. Physik. Chem., 5, 3

Bancelin, 1911: Bancelin, M., Comp. Rend., 152, 1382

Barnes, 1980: Barnes, H A, Dispersion Rheology - a survey of industrial problems and academic progress, Royal Society of Chemistry's Industrial Division, London, UK

Wakeman, 1975: Wakeman, R., Powder. Tech., 11, 297 – 299

Barnes, 2000: Barnes, H A, Handbook of elementary Rheology, Chapter 15, Institute of Non-Newtonian Fluid Mechanics, University of Wales, Wales, UK

Barnes et al., 1989: Barnes, H.A; Hutton, J.F; Walters, K, 'An Introduction to Rheology', Elsevier, Amsterdam, Netherland

Lund et al., 1997: A. Lund, O. Urdahl, O. Lier, L.H. Gjertsen, T. Jakobsen and J.A. Støvneng, Proc. 7nd Int. Offshore and Polar Eng. Conf., Honolulu, USA, May 25-30, 1997, p. 110.

Sugaya and Mori, 1996: M. Sugaya and Y.H. Mori, Chem. Eng. Sci., 51 (1996) 3505-3517.

Sloan and Koh, 2008: E. D. Sloan, Carolyn A. Koh, Clathrate Hydrates of Natural Gases, Third Edition, CRC Press Taylor & Francis Group, London, UK

Lund and Larsen, 2000: A. Lund, R. Larsen, Conversion of Water to Hydrate Particles – Theory and Application, The 14th Symposium on Thermophysical Properties, Boulder, Colorado, US

APPENDICES

APPENDIX A: List of Entries in the item structure

Struct	Entry	Type	Description	Unit
param				
	Comment	Text	Written to output file	
	outputfile	Text	Output written to this file	
	Tinf	Real	Sea temperature, deg C	deg C
	Tref	Real	Reference temperature for Enthalpy calc.	deg C
	Cpwater	Real	Heat capacity of water	J/kg.K
	Cphydrate	Real	hydrate	J/kg.K
	CpLHC	Real	light hydrocarbons	J/kg.K
	CpHHC	Real	heavy hydrocarbons	J/kg.K
	dHfhydrate	Real	Heat of formation, hydrate	J/kg
	dHfwater	Real	water	J/kg
	dHfLHC	Real	light hydrocarbons	J/kg
	hydratefun	Function handle	Thydrate=hydratetemp(p) should return hydrate curve.	
	rxfun	Function handle	Function for reaction rate	
	rho	1x4 real vector	Densities of hydrate,water,LHC,HHC.	kg/m3
	dp	Real	Mean particle size of hydrate	m
	x	Real	x kg vann + y kg LHC <--> (x+y) kg hydrat	kg
	y	Real	Ditto	kg
item{i} when item i is a source				
	name	Text	Name of the unit	
	type	Text	='source'	
	massflow	Real	Mass flow	kg/s
	Ncomp	Integer	Number of components (Must be 4 in the present version of the simulator)	
	x	1x4 real vector	Mass fractions	
	T	Real	Stream temperature	deg C
	dHf	Real	Heat of formation of stream	J/kg
	Cp	1x4 real vector	Heat capacity of stream	J/kg.K
item{i} when item i is a mixer				
	name	Text	Name of the unit	
	type	Text	='mixer'	
	upstream1	1x2 real vector	Inlet stream 1. E.g. item{3}.upstream1=[1 A]	
	upstream2	1x2 real vector	Inlet stream 2.	
item{i} when item i is a plug flow reactor				
	name	Text	Name of the unit	
	type	Text	='reactor'	
	upstream1	1x2 real vector	Inlet stream. E.g. item{4}.upstream1=[3 A]	
	L	Real	Length of reactor	m
	area	Real	Cross sectional pipe area	m2
	Ua	Real	U*A per meter pipe length	W/m.K
	p	Real	Pipe pressure	bar
item{i} when item i is a pipe				
	name	Text	Name of the unit	
	type	Text	='pipe'	
	upstream1	1x2 real vector	Inlet stream. E.g. item{5}.upstream1=[4 A]	
	L	Real	Length of reactor	m
	area	Real	Cross sectional pipe area	m2
	Ua	Real	U*A per meter pipe length	W/m.K
item{i} when item i is a splitter				
	name	Text	Name of the unit	
	type	Text	='splitter'	
	upstream1	1x2 real vector	Inlet stream. E.g. item{6}.upstream1=[5 A]	
	alpha	Real	Mass fraction to output A	

APPENDIX B: Input File example

```
% Input file for hydrate reactor
%14/8-01 John Morud

%Units:
h    = 3600;     %s (Definer enhet)
kg   = 1;
cm   = 0.01;     %m
mm   = 0.001;    %m
inch = 2.54*cm;
ft   = 0.3048;   %m
s    = 1;
cP   = 0.001;    %SI-enheter
psi=6.8948e3;    %Pa
scf_STB=1/5.617; %Sm3/m3
Sm3=42.292;      %mol   (ISO)

%Input parameters
param.Comment='CF, 1" loop, 10% vann, 1 m/s, 60 C brønnstrøm, 1:1, visk 1 cP
';    %Written to output file
param.outputfile='OutputTestFile.txt';          %Name output file
param.Tinf=4;                                   %Input cooling water
temperature/Sea temperature, deg C
param.Tref=20;                                  %Reference temperature for
Enthalpy calc.
param.Cpwater=4200;                             %J/kg.K
param.Cphydrate=2200;                           %J/kg.K
param.CpLHC=4062;                               %J/kg.K. Cp for light
hydrocarbons
param.CpHHC=1760;                               %J/kg.KCp for heavy
hydrocarbons
param.dHfhydrate=-477.4e3;                      %J/kg
param.dHfwater=0;                               %J/kg
param.dHfLHC=0;                                 %J/kgHeat of formation for
light hydrocarbons
param.hydratefun=@hydratetempmal;               %Thydrate=hydratetemp(p)
returns hydrate curve.
param.rxfun=@reacratemal;                       %function for reaction rate
param.viscfun=@viscosity;                       %function for viscosity
(Pa.s)
param.Moodyfun=@slurryfriction;                 %function for Moody
friction factor
param.hslurryfun=@hslurry;                      %function for heat transfer
coeff in slurry [W/m2.K]
param.Ucoolandsteelfun=@Ucoolandsteel;          %function for pipe and
cooling liquid heat transf coeff
param.plugfloweqsfun=@plugfloweqs;
param.rho=[950 1000 299 864];                   %Densities of hydrate water
LHC HHC.
param.dp=0.1e-3;                                %m mean particle size of
hydrate
param.x=4.8; param.y=1;                         %x kg vann + y kg LHC <-->
(x+y) kg hydrat
```

```
param.gor=500*scf_STB;                              %GOR in Sm3/m3
param.SG=18.5/28.8;                                 %Specific gas gravity

%-------------------------------------------------------------------------
%   VISCOSITY DATA PARAMETERS

param.Tlow_visc   = 4;            %Degree Celsius
param.Thigh_visc  = 20;           %Degree Celsius
param.visc_lowT   = 1*cP;         %Input in centi Poise
param.visc_highT  = 0.67*cP;      %Input in centi Poise
param.weight_frac_coeff = 0.1161; % Assuming relative viscosity depends on
weight fraction as exp(A*wt%)

%-------------------------------------------------------------------------
%   COOLING SYSTEM PARAMETERS
param.Ucool   = 1.0;
param.kcool   = 0.44;
param.kwall   = 40;
param.mucool  = 0.0025;
param.Cpcool  = 3825;
param.rhocool = 1030;

param.do  = 33.4*mm;
param.ro  = param.do/2;           %1" pipe
param.di  = param.do-2*(4.55*mm); %wall thickness
param.ri  = param.di/2;
param.area= pi*param.di^2/4;      %inside cross sect. area
param.dij = 2.5*inch;             %ID cooling jacket

mCpwater = param.rhocool*param.Ucool*pi*0.25*(param.dij^2 -
param.do^2)*param.Cpcool;

%Sources:
flowmultiplier = 1;
i=1;
%item 1
item{i}.name='Hydratstrøm';
item{i}.type='source';
item{i}.massflow=flowmultiplier*0.0145*41.56*1000*kg/h;
%kg/s
item{i}.Ncomp=4;
% # of components
item{i}.x=[0.1 0 0.12     0.78]'/1;
%Mass fractions
item{i}.T=4;
% deg C
item{i}.dHf=item{i}.x(1)*param.dHfhydrate;
% Heat of formation of stream
item{i}.Cp=item{i}.x'*[param.Cphydrate param.Cpwater param.CpLHC
param.CpHHC]';% Heat capacity of stream, J/kg.K
item{i}.P=109.e5;
%Pa pressure
```

```
i=2;                                                    %item 2
item{i}.name='Brønnstrøm';
item{i}.type='source';
item{i}.massflow=flowmultiplier*0.0145*41.56*1000*kg/h;  %kg/s
item{i}.Ncomp=4;                                        % # of components
item{i}.x=[0 0.083 0.134 0.783]'/1;                     %Mass frac of
hydrate, water, light HC and heavy HC
%item{i}.T=40;                                          % deg C
item{i}.T=60;                                           % deg C
item{i}.dHf=item{i}.x(1)*param.dHfhydrate;              %Heat of formation
item{i}.Cp=item{i}.x'*[param.Cphydrate param.Cpwater param.CpLHC
param.CpHHC]';    % Heat capacity, J/kg.K
item{i}.P=109.e5;                                       %Pa pressure

%-------------------------------------------------------------------------
%Mixers:
i=3;
item{i}.name='Blandesone';
item{i}.type='mixer';
item{i}.upstream1=[1 A];
item{i}.upstream2=[2 A];

% %-------------------------------------------------------------------------
% %Splitters:
% i=4;
% item{i}.name='';
% item{i}.type='splitter';
% item{i}.upstream1=[3 A];
% item{i}.alpha=0.4; %Mass fraction to output A
%
% %-------------------------------------------------------------------------
%Pipes:
%i=4;
%item{i}.name='Rørledning';
%item{i}.type='pipe';
%item{i}.upstream1=[3 A];
%item{i}.L=1500;   %pipe length
%item{i}.area=0.05;   %m2 cross sectional area
%item{i}.Ua=20;       %UA per meter pipe
%
% %-------------------------------------------------------------------------
%Reactors
%
%------------------------
%Preliminary calculation of heat transfer
%units:
cm=0.01;     %m
mm=0.001;    %m
inch=2.54*cm;
ft=0.3048;   %m
s=1;
cP=0.001; %SI-enheter
```

```
%data (Må finne data for oljer....)
koil=0.1407; %W/m.K
muoil=(0.115*0.0277+(1-0.115)*5.911)*cP;
Cpoil=0.115*4062+(1-0.115)*1760;
Proil=muoil*Cpoil/koil;
rhooil=0.115*100+(1-0.115)*864;
v=1;

kwater=0.6;
muwater=1.e-3;
Cpwater=4200;
Prwater=muwater*Cpwater/kwater;
rhowater=1000;
vsea=2*ft/s; %Sea current

%Heat transfer
do=33.4*mm; ro=do/2;      %1" O.D. pipe
di=do-2*4.55*mm; ri=di/2; % wall thickness
area=pi*di^2/4;           %inside cross sect. area

hfoul = 2840;                                      %W/m2.K muddy water
Reoil = v*di*rhooil/muoil;                         %Reynoldsnumber inside pipe
hi    = 0.0255*(koil/di)*Reoil^0.8*Proil^0.4;      %inner heat transfer coeff
kwall = 65.0;                                      %W/m.K plain carbon steel
Resea = vsea*do*rhowater/muwater;                  %Reynoldsnumber on outside
of pipe
hsea  = 0.28*(kwater/do)*Resea^0.56*Prwater^0.3; %Heat transfer coefficient
on sea side of pipe.

Rtot=1/(hsea*2*pi*ro)+1/(hfoul*2*pi*ro)+log(ro/ri)/(2*pi*kwall)+1/(hi*2*pi*r
i); %Heat transfer resistance per m.
Uatot=1/Rtot;

%-------------------------------------------------------------------------
%Definitions for slurry friction factors and heat transfer
%Correlation for Drag coefficient at terminal setling velocity for slurry
particles
Abraham   = 1;
Karamaner = 2;
%Correlation for friction factor calculation
Haaland   = 1;
JCM       = 2;
Darcy     = 1;
Fanning   = 2;
slurry1.epsilon = 0.0;    %pipe roughness
slurry1.dpart = param.dp; %particle size
slurry1.rhos  = 900;      %slurry particle density
surry1.type = [Abraham JCM Darcy ];

slurry1.kslurry=koil;

%-------------------------------------------------------------------------
% i=4;
% item{i}.name='HydratreaktorSection0m';
```

```
% item{i}.type='reactor';
% item{i}.upstream1=[3 A];  %upstream unit
% item{i}.L=2;              %length of reactor
% item{i}.area=area;        %m2 cross sectional area
% item{i}.Ua=Uatot;         %UA per meter (Guess only)
% item{i}.UaWaterAndSteel=Uatot; %Ua per meter for water and steel (i.e.
without slurry friction factor)
% item{i}.p=109;            %bar (Used for hydrate curve. Not pressure
drop!)
% item{i}.slurry=slurry1;

DeltaL=18;           %meter
Reference=0;         %Mark the position where the last item ended.

i=4;
item{i}.name=['HeatExchanger Start:' num2str(Reference) ' m'];
Reference=Reference+DeltaL;
item{i}.type='HXreactor';
item{i}.upstream1=[i-1 A];      %upstream unit
item{i}.L=18;                   %length of reactor
item{i}.area=area;              %m2 cross sectional area
item{i}.Ua=Uatot;               %UA per meter (Guess only)
item{i}.UaWaterAndSteel=Uatot;  %Ua per meter for water and steel (i.e.
without slurry friction factor)
item{i}.p=109;                  %bar (Used for hydrate curve, not pressure
drop)
item{i}.mCpWater=mCpwater;      %mdot*Cp for water            (* NEW)
item{i}.Twater=1;               %C temperature at inlet       (* NEW)
item{i}.slurry=slurry1;

%Add more:
for i=4+(1:12)
    item{i}.name=['HeatExchanger Start:' num2str(Reference) ' m'];
Reference=Reference+DeltaL;
        item{i}.type='HXreactor';
        item{i}.upstream1=[i-1 A];       %upstream unit
        item{i}.L=DeltaL;                %length of reactor (DeltaL)
        item{i}.area=area;               %m2 cross sectional area
    item{i}.Ua=Uatot;                %UA per meter (Guess only)
    item{i}.UaWaterAndSteel=Uatot;   %Ua per meter for water and steel (i.e.
without slurry friction factor)
        item{i}.p=109;                   %bar (Used for hydrate curve. Not
pressure drop!)
        item{i}.mCpWater=mCpwater;       %mdot*Cp for water       (* NEW)
        item{i}.Twater=1;                %C temperature at inlet       (*
NEW)
    item{i}.slurry=slurry1;
end
```

Published with MATLAB® R2016a

APPENDIX C: Output File example

```
************************************************************
PROGRAM:       H Y D R A T E  S I M U L A T O R  FOR MATLAB
AUTHORS:              J. Morud and P. Skjetne
                  SINTEF Materials and Chemistry, NORWAY
                            CONWHYP ver 13
************************************************************

            S I M U L A T I O N   R E S U L T S
            ===================================

DATE:     01-May-2017        TIME: 14:16
CASEFILE: InputTestFile

COMMENTS:
  CF, 1" loop, 10% vann, 1 m/s, 60 C brønnstrøm, 1:1, visk 1 cP

****************** SPECIFIED INPUT DATA **********************

PHYSICAL PARAMETERS:
Sea temperature:                      4.00 [C]
Reference temp. for enthalpy:        20.00 [C]

Heat capacities (Cp):
     hydrate:                      2200.00 [J/kg.K]
     water:                        4200.00 [J/kg.K]
     light hydrocarbon:            4062.00 [J/kg.K]
     heavy hydrocarbon:            1760.00 [J/kg.K]

Heat of formation (dHf):
     hydrate:                     -477400.00 [J/kg]
     water:                          0.00 [J/kg]
     light hydrocarbon:              0.00 [J/kg]

Function for hydrate curve:     hydratetempmal
Function for reaction rate:     reacratemal

Densities:
     hydrate:                      950.00 [kg/m3]
     water  :                      1000.00 [kg/m3]
     light hydrocarbon:            299.00 [kg/m3]
     heavy hydrocarbon:            864.00 [kg/m3]

Mean hydrate particle size  :        0.10 [mm]
Reaction rate equation      :
 4.80 [kg water] + 1.00 [kg light HC] <==> 5.80 [kg hydrate]
Page Break
************* UNITS AND STREAMS ************************

Item number                 :      1
Item name                   :      Hydratstrøm
Item type                   :      source
Mass flow                   :      0.17 [kg/s]  (  0.60 [ton/h])

Mass fractions:
      hydrate               :        0.12
      water                 :        0.00
      light HC              :        0.12
      heavy HC              :        0.76
```

```
Temperature                 :        4.00 [C]
Pressure                    :    10900000.00 [Pa]
Total heat of formation     :      -57288.00 [J/kg]
Total Cp                    :     2089.04 [J(kg.K]

-------------------------------------------------------------


Item number                 :     2
Item name                   :     Brønnstrøm
Item type                   :     source
Mass flow                   :       0.17 [kg/s]  (  0.60 [ton/h])

Mass fractions:
      hydrate               :       0.00
      water                 :       0.08
      light HC              :       0.13
      heavy HC              :       0.78

Temperature                 :      60.00 [C]
Pressure                    :    10900000.00 [Pa]
Total heat of formation     :      -0.00 [J/kg]
Total Cp                    :     2270.99 [J(kg.K]

-------------------------------------------------------------


Item number                 :     3
Item name                   :     Blandesone
Item type                   :     mixer
Upstream unit 1             :     item 1 outlet 1 (Hydratstrøm)
Upstream unit 2             :     item 2 outlet 1 (Brønnstrøm)

Outlet mass flow            :       0.33 [kg/s]  (  1.21 [ton/h])
Outlet mass fractions       :
      hydrate               :       0.06
      water                 :       0.04
      light HC              :       0.13
      heavy HC              :       0.77

Outlet temperature          :      33.17 [C]
Outlet pressure             :    10900000.00 [Pa]
Total heat of formation     :     -28644.00 [J/kg]
Total Cp                    :     2180.01 [J(kg.K]

-------------------------------------------------------------


Item number                 :     4
Itemname                    :     HeatExchanger Start:0 m

Item type                   :     HXreactor
Upstream unit               :     item 3 outlet 1 (Blandesone)

Pipe length                 :      18.00 [m]
Heat transfer coefficient   :      49.82 [W/m.K]
Operating pressure          :     109.00 [bar]
Cross sectional area        :      0.000 [m2]
Fluid velocity              :       1.03 [m/s]
Reynolds number             :      10424 [-]
Fluid viscosity             :     1.6829e-03 [Pa.s]
```

```
Water depleted at position  :       [m]
Temperature at that point   :       [C]

Outlet mass flow            :        0.33 [kg/s]  (  1.21 [ton/h])

Inlet mass fractions        :
      hydrate               :        0.06
      water                 :        0.04
      light HC              :        0.13
      heavy HC              :        0.77

Outlet mass fractions       :
      hydrate               :        0.06
      water                 :        0.04
      light HC              :        0.13
      heavy HC              :        0.77

Inlet temperature           :       33.17 [C]
Outlet temperature          :       10.81 [C]
Outlet pressure             :    10892075.64 [Pa]
Outlet heat of formation    :      -28644.00 [J/kg]
Outlet Cp                   :      2180.01 [J/kg.K]

Cooling water                 :
      M*Cp                    :     9025.03 [W/K]
      Inlet water temperature :       1.00 [C]
      Outlet water temperature:       2.81 [C]
      Duty                    :    16315.31 [W]
```

APPENDIX D: Viscosity function

```
function mu=viscosity2(p,T,x,par)

T0   = par.Tlow_visc + 273.15; %Temp input in [C] used in [K]
T1   = par.Thigh_visc + 273.15;%Temp input in [C] used in [K]
eta0 = par.visc_lowT;  %Assumed viscosity at T0 [K] in Pa.s
eta1 = par.visc_highT; %Assumed viscosity at T1 [K] in Pa.s

B = ((T0*T1)/(T0-T1))*log10( (eta1/eta0));
A = log10(eta0) - B/T0;

mu=(10.^(A + B/T))*(1-x(1)/par.MPF)^-2;%Viscosity calculation using K-D
equation
```

Published with MATLAB® R2016a

APPENDIX E: Viscosity profile script

```
[streamtable,item]=HydrateMain('InputTestFile',2);

Test1 = zeros(2,length(item)); %Creating empty vector for storage of length
and viscosity data
for i = 4:length(item) %Storing length and viscosity data
    Test1(1,i)=item{1,i}.mu*1000;
    Test1(2,i)=Test1(2,i-1)+item{1,i}.L;

end

%Repeating process for more input files:
[streamtable2,item2]=HydrateMain('InputTestFile2',2);
Test2 = zeros(2,length(item2));
for i = 4:length(item2)
    Test2(1,i)=item2{1,i}.mu*1000;
    Test2(2,i)=Test2(2,i-1)+item2{1,i}.L;

end

[streamtable3,item3]=HydrateMain('InputTestFile3',2);
Test3 = zeros(2,length(item3));
for i = 4:length(item3)
    Test3(1,i)=item3{1,i}.mu*1000;
    Test3(2,i)=Test3(2,i-1)+item3{1,i}.L;

end

[streamtable4,item4]=HydrateMain('InputTestFile4',2);
Test4 = zeros(2,length(item4));
for i = 4:length(item4)
    Test4(1,i)=item4{1,i}.mu*1000;
    Test4(2,i)=Test4(2,i-1)+item4{1,i}.L;

end

%Configuring plots
linewidth = 2;
plot(Test1(2,4:length(item)),Test1(1,4:length(item)),'LineWidth',linewidth);
hold on
plot(Test2(2,4:length(item)),Test2(1,4:length(item)),'LineWidth',linewidth);
plot(Test3(2,4:length(item)),Test3(1,4:length(item)),'LineWidth',linewidth);
plot(Test4(2,4:length(item)),Test4(1,4:length(item)),'LineWidth',linewidth);
xlabel('Position [m]','fontsize',16,'fontweight','bold');
ylabel('Viscosity [cP]','fontsize',16,'fontweight','bold');
legend('Legend1','Legend2','Legend3','Legend4');
```

Published with MATLAB® R2016a

APPENDIX F: Pressure profile script

```
[streamtable,item]=HydrateMain('InputTestFile',2);

Test1 = zeros(2,length(item)); %Creating empty vector for storage of length
and pressure data
for i = 4:length(item) %Storing length and pressure data
    Test1(1,i)=streamtable{i,1}.P/10^5; %From Pa to bar
    Test1(2,i)=Test1(2,i-1)+item{1,i}.L;

end

%Repeating process for more input files:
[streamtable2,item2]=HydrateMain('InputTestFile2',2);
Test2 = zeros(2,length(item2));
for i = 4:length(item2)
    Test2(1,i)=streamtable2{i,1}.P/10^5;
    Test2(2,i)=Test2(2,i-1)+item2{1,i}.L;

end

[streamtable3,item3]=HydrateMain('InputTestFile3',2);
Test3 = zeros(2,length(item3));
for i = 4:length(item3)
    Test3(1,i)=streamtable3{i,1}.P/10^5;
    Test3(2,i)=Test3(2,i-1)+item3{1,i}.L;

end

[streamtable4,item4]=HydrateMain('InputTestFile4',2);
Test4 = zeros(2,length(item4));
for i = 4:length(item4)
    Test4(1,i)=streamtable4{i,1}.P/10^5;
    Test4(2,i)=Test4(2,i-1)+item4{1,i}.L;

end

%Configuring plots
linewidth = 1.0;
plot(Test1(2,4:length(item)),Test1(1,4:length(item)),'LineWidth',linewidth);
hold on
plot(Test2(2,4:length(item)),Test2(1,4:length(item)),'LineWidth',linewidth);
plot(Test3(2,4:length(item)),Test3(1,4:length(item)),'LineWidth',linewidth);
plot(Test4(2,4:length(item)),Test4(1,4:length(item)),'LineWidth',linewidth);
xlabel('Position [m]','fontsize',16,'fontweight','bold');
ylabel('Pressure [bar]','fontsize',16,'fontweight','bold');
legend('Legend1','Legend2','Legend3','Legend4');
```

Published with MATLAB® R2016a

APPENDIX G: Slurry friction function

```
function f=slurryfriction(v, rhof, muf, D, epsi, Cpart, dpart, rhos, Re_lam,
types)
%v     [m/s] slurry superficial velocity in pipe
%rhof  [kg/m3] density of carrier fluid
%muf   [Pas]   viscosity of carrier fluid
%D     [m]     pipe diameter
%epsi  [mm]    pipe wall roughness
%Cpart [-]     volume fraction of slurry particles [0,1]
%dpart [m]     diameter of slurry particles
%rhos  [kg/m3] density of slurry particles
%types [-]  integer vector
%      (1)  integer selecting Abraham (=1) or Karamaner (=2) approx for
%           calculating settling velocity of slurry particles.
%      (2)  integer determining which type of explicit friction factor
approximation
%           to use Haaland (=1) JCM (=2)
%      (3)  integer determining whether to return a Darcy or Fanning
%           friction factor. Darcy (=1) Fanning (=2)
%
%
%NOTE the calling routine is expecting a Darcy friction factor. Inside this
routine
%all correlations are based on the Fanning friction factor, thus the final
friction factor
%should be multiplied by 4. This is done by multiplying with the constant
multiplier.
%

if types(3) == 1
    multiplier = 4.0;
else
    multiplier = 1.0;
end

%Polynomal coefficients and exponents
c0 = [12.13
      107.1
      30.11
      8.538];
c1 = [0.7389
      1.018
      0.868
      0.5024];
c2 = [0.7717
      1.046
      1.200
      1.428];
c3 = [-0.4054
      -0.4213
      -0.1677
       0.1516];
c4 = [-1.096
      -1.354
```

```
      -0.6938
      -0.3531];

% Pre-calculate some variables:

gravity = 9.81;
Re      = rhof*v*D/muf;
Fr      = v*v/(gravity*D*(rhos/rhof -1.0));
Cdstar  = dragcoeff(dpart, rhof, rhos, muf, types(1));
fw      = fanningfriction(Re, epsi, D, Re_lam, types(2));


% Determine flow regime of the slurry
Rab    = slurrystate(Cpart, fw, Cdstar, Fr);

% Calculate slurry friction factor

j = Rab + 1;
fs = fw + c0(j)*Cpart^c1(j)*fw^c2(j)*Cdstar^c3(j)*Fr^c4(j);

f = multiplier*[fs fw j/multiplier];
```

Published with MATLAB® R2016a

APPENDIX H: Drag coefficient function

```
function Cdstar = dragcoeff(dp, rhof, rhos, muf, dtype)
Abraham   = 1;
Karamaner = 2;
gravity   = 9.81;
phi1star = (4/3*(rhos-rhof)*rhof*gravity/muf^2 )*dp^3;
if(dtype == Karamaner)
        Cdstar = (432/phi1star)*(1+0.0470*phi1star^(2/3)) +
0.517/(1+154*phi1star^(-1/3));
elseif(dtype == Abraham)
        dpstar = phi1star^(1/3);
        vtstar = (20.52/dpstar)*( sqrt(1+0.0921*dpstar^(3/2)) - 1)^(2.0);
        Cdstar = dpstar/(vtstar^2);
else
        error(' The variable ''dtype'' must have the value 1 or 2');
end
```

Published with MATLAB® R2016a

APPENDIX I: Reading ternary diagrams

Ternary diagrams may look confusing at first, but are a convenient way of representing a systems where three components/phases are present, and how the system behaves for a given composition. The figure below shows a typical ternary diagram template for the three classes:

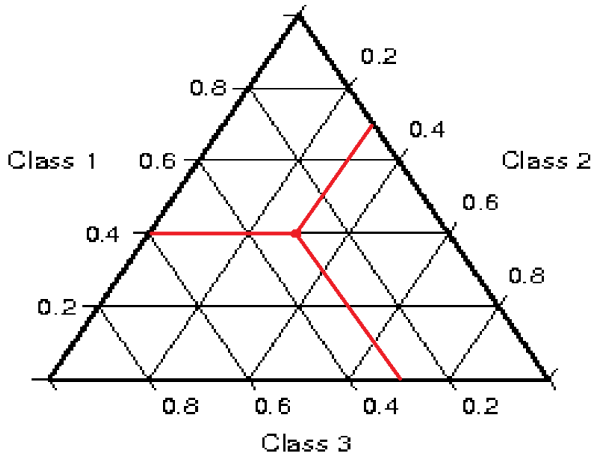

Each of the three edges around the triangle shows the fraction of each class. For instance, for Class 1, we have a volume fraction of 0% in the low left corner, and 100% in the top of the triangle. Similarly, class 2 has a volume fraction of 0% in the top, and 100% in the lower right corner. Class 3 has 0% in the lower right corner and 100% in the lower left corner.

A convenient way of using the diagram is to draw up “help-lines” inside the triangle. These are the thinner lines we see that are parallel to the edges of the triangle. We can then mark any point inside the diagram, draw three lines to the edges of the triangle, and thereby read the volume fraction of each of the components. For the red dot in this figure, three lines are drawn, yielding a composition of 40% class 1, 30% class 2 and 30% class 3. This point (or region in some cases) is then connected to a parameter, such as viscosity in the case of this paper.

APPENDIX J: Sensitivity analysis script

```
%Sensitivity Analysis for hydrate volume and maximum packing fraction

HVF = 5:5:40; %Hydrate volume fraction vector
MPF = 62:2:72; %Maximum packing fraction vector
Viscosity = zeros(length(MPF),length(HVF)); %Creating empty viscosity matrix

%Performing calculations
for i = 1:length(MPF)
    for j = 1:length(HVF)
        Viscosity(i,j) = (1-HVF(j)/MPF(i))^-2;
    end
end

%Setting up the surface plot
surf(HVF,MPF,Viscosity);
xlabel('HVF','fontsize',16,'fontweight','bold');
ylabel('MPF','fontsize',16,'fontweight','bold');
zlabel('Viscosity','fontsize',16,'fontweight','bold');
```